Thin-Walled Structures 170 (2022) 108638

Contents lists available at ScienceDirect

Thin-Walled Structures

journal homepage: www.elsevier.com/locate/tws

Full length article

Buckling resistance of concrete-filled cold-formed steel (CF-CFS) built-up short columns under compression

Rohola Rahnavard *, Hélder D. Craveiro *, Rui A. Simões, Luís Laím, Aldina Santiago

University of Coimbra, ISISE, Department of Civil Engineering, Coimbra, Portugal

ARTICLE INFO

Keywords:
Concrete-filled
Cold-formed steel
Built-up section
Composite column
Buckling

ABSTRACT

The steel–concrete composite columns (SCCC) are widely used in the construction sector. The buckling phenomenon of the steel part (especially thin-walled steel) of the SCCC due to compressive loading is the governing characteristic of these columns. The present paper reports an experimental and numerical study on the compressive behavior of innovative concrete-filled (CF) closed built-up cold-formed steel (CFS) columns to investigate the applicability of EN 1994-1-1 for the prediction of the buckling resistance. Twelve CF-CFS short columns were tested. The finite element (FE) design, test setup, procedure, and results, including the load-carrying capacities, load–deformation, and buckling modes, were fully reported. Additionally, the numerical results and EN 1994-1-1 predictions were compared assessing the validity of the EN 1994-1-1 formulations for the estimation of the contributions of each component. Since the closed built-up cross-sections are composed of Class 4 individual cross-sections, both gross and effective sectional areas were considered to estimate the steel contribution to the overall resistance of the composite columns. Based on the FE results it was observed that using the gross area the EN 1994-1-1 formulation overestimates the steel contribution and underestimates it when the effective area is used. Therefore, a modification was proposed for determining the effective cross-sectional areas of Class 4 closed built-up CFS cross-sections, by considering the overlapping plates, fastener positioning, and the concrete encasement of the individual plate elements resulting in a close agreement between the proposed methodology and experimental results.

1. Introduction

Due to the appropriate composite action between the steel sections and concrete, concrete-filled steel tubular columns are becoming increasingly used in various structures. Extensive experimental and analytical studies have been conducted to understand the behavior of the composite columns [1–10]. The use of steel box sections filled with concrete for columns has many advantages. The concrete core can contribute to mitigating premature local buckling phenomena on the tubular steel section. Also, the confinement of the concrete by the steel section can enhance the development of the compressive strength of the concrete. In addition, formworks are not required for concrete casting. As a result, these composite columns provide higher strength and rigidity in an economical and environmentally friendly manner, as well as improved fire resistance behavior. Different design codes including Australian standard AS 5100 (2004) [11], American specification ANSI/AISC [12], Chinese codes (DBJ/T 13-51-2010 [13] and JGJ 138-2016 [14]), and EN 1994-1-1 [15] address specifically the subject of concrete-filled composite columns.

A relevant part of previous studies was focused on stainless steel composite columns [16–28]. Hassanein et al. [29–38] investigated the axial and flexural behavior of circular concrete-filled stainless steel tubular columns using experimental and numerical tools. They used lean duplex stainless steel as the external tube. They also studied the effects of the slenderness of concrete-filled dual steel tubular columns on their buckling behavior. They compared their results with analytical predictions obtained from DBJ/T 13-51 [13] and EN 1994-1-1 [15], concluding that analytical predictions are slightly unconservative based on EN 1994-1-1 [15] for intermediate-length columns. Considering buckling curve *d* instead of curve *c* [15] provided safer predictions. The effect of confinement of stiffened and unstiffened concrete-filled stainless steel tubular short columns was investigated by Dabon et al. [39, 40] resulting in highly conservative code predictions (American specification ANSI/AISC [12] and EN 1994-1-1 [15]). Xiong et al. [41–43] investigated the axial and flexural performance of short and long concrete-filled steel tubes with high and ultra-high-strength materials. Their results showed that EN 1994-1-1 [15] provides conservative results if the confinement effect is not considered and if Class 3 steel sections are not used.

Kazemzadeh et al. [44–46] investigated axial slenderness limits and the local and post-local buckling for concrete-filled stainless steel

* Corresponding authors.
E-mail addresses: rahnavard@uc.pt, rahnavard1990@gmail.com (R. Rahnavard), heldercraveiro.eng@uc.pt (H.D. Craveiro).

https://doi.org/10.1016/j.tws.2021.108638
Received 29 April 2021; Received in revised form 6 September 2021; Accepted 1 November 2021
Available online 20 November 2021

Notation

A_a	Cross-sectional area of the structural steel section
A_s	Area of the steel reinforcement
A_c	Cross-sectional area of concrete
A_{eff}	Effective cross-sectional area of the structural steel section
E_s	Modulus of elasticity of steel
$\overline{E}_s$	Average value of modulus of elasticity of the steel material
$\overline{E}_{cm}$	Average value of modulus of elasticity of concrete material
$E_{c,eff}$	Reduced value of modulus of elasticity of concrete material
D	Density
$\overline{D}$	Average value of density
$P_{u,test}$	Axial capacity of the column based on experimental test
$P_{average,test}$	Average value of Axial capacity of the column based on experimental test
W_{comp}	Weight of the composite column
P/W_{comp}	Load–weight ratio
P_{max}	Maximum axial load based on experimental test
$N_{pl,Rd}$	Plastic resistance of the composite column section
$N_{b,Rd}$	The design buckling load of the composite column member
P_{CFS}	CFS contribution on the axial load-bearing capacity of composite column based on finite element method
P_{CF}	Concrete-filled contribution on the axial load-bearing capacity of composite column based on finite element method
P_{CF-CFS}	Axial load-bearing capacity of concrete-filled cold-formed steel composite column based on finite element method
P_{CFSb}	Axial load-bearing capacity of CFS built-up column based on finite element method
N_{cr}	Elastic buckling force
$N_{cr,F}$	Elastic flexural buckling force
$N_{cr,T}$	Elastic torsional buckling force
$N_{cr,TF}$	Elastic torsional-flexural buckling force
I_s	Second moment of area of the stiffener
I_a	Second moments of area of the structural steel section
I_s	Second moments of area of the un-cracked concrete section
I_c	Second moments of area of the reinforcement for the bending plane
L_e	Effective length of column
L^{el}	The smallest element size
EI_{eff}	Effective flexural stiffness
K	Spring stiffness per unit length of a stiffener
f_y	Yield strength
b	Width of a cross-section, plate width
b_e, b_{eff}	Effective width of a cross-section, effective plate width
c	Lip length of a cross-section
c_e	Effective lip length of a cross-section
c_d	The wave speed of the material
h	Height of a cross-section
h_e	Effective height of a cross-section
k_σ	Buckling factor depending on the stress distribution and boundary conditions of the plate
f_{yd}	Design value of the yield strength of structural steel
Δt	Scaling factor
t	Plate thickness
r	Radius of gyration of a cross-section
k_e	Correction factor
δ	Steel contribution ratio
Φ	Safety factors for the available axial strength based on the Limit States Design (LSD)
φ_t	Creep coefficient
α	Imperfection factor
λ	Slenderness factor
$\overline{\lambda}$	Relative slenderness
ν	Poisson's ratio in elastic stage
ρ	Reduction factor for plate buckling
σ_{cr}	Elastic critical plate buckling stress
$\sigma_{cr,s}$	Elastic critical buckling stress for an edge stiffener
χ	Reduction factor for relevant buckling mode
χ_d	Reduction factor for the distortional buckling resistance
β	Reliability index

composite columns (concrete-filled box, concrete-filled circular, and partially encased I-sections). Maximum local amplitude imperfections of $b/450$ and $b_f/120$ were proposed for fabricated box sections. It was observed that for short concrete-filled steel tubular columns, local buckling is the governing failure mode. Han et al. [47–51] investigated short and slender concrete-filled stainless steel tubular columns using experimental tests and the finite element method. Failure modes, load bearing capacity, and buckling modes were extensively compared. Also, the use of carbon steel and stainless steel in concrete-filled columns was assessed. Stainless steel composite columns showed a more ductile behavior with higher post-buckling strength comparing to those composite columns with carbon steel tubes. Ellobody [52–54] performed several experimental tests on concrete-filled cold-formed high strength stainless steel tube columns and compared the results with design predictions according to the EN 1994-1-1 [15] and Australian Standards AS3600 & AS4100 [20]. It was observed that design predictions according to the Australian/New Zealand specifications [20] presented conservative results, whereas the European standard presented in general unconservative results. Circular and square concrete-filled stainless steel columns were investigated by Lam and Gardner [55] and Giakoumelis and Lam [56]. A total of 16 stub columns were tested and the results were compared with the EN 1994-1-1 [15] and the Continuous Strength Method (CSM) [57]. The CSM provided the closest prediction since it has provided a more precise assessment of the steel contribution. Concrete-filled double-skin tubular cross-sections with stainless steel tubes were also investigated by Fangying et al. [58–60]. The authors recommended the use of effective compressive strength to improve the accuracy of design predictions.

Built-up cold-formed steel sections combining several individual shapes are extensively used in the Light-Steel Framing (LSF) industry

Table 1
Specimens details.

Column configuration	Length (mm)	CFS profiles			Fasteners distance (mm)			Fasteners spacing (mm)	A_a (mm^2)	A_c (mm^2)
		C	U	Σ	h_1	h_2	h_3			
R-2C + 2U	1050	2	2	–	39	23	–	237.5	1485	12 121.5
S-2C + 2U	1050	2	2	–	–	21.5	–	237.5	1485	21 720.0
R-2Σ + 2U	1050	–	2	2	–	21.5	11.5	237.5	1540	8912.8
S-2Σ + 2U	1050	–	2	2	–	21.5	11.5	237.5	1540	18 307.1

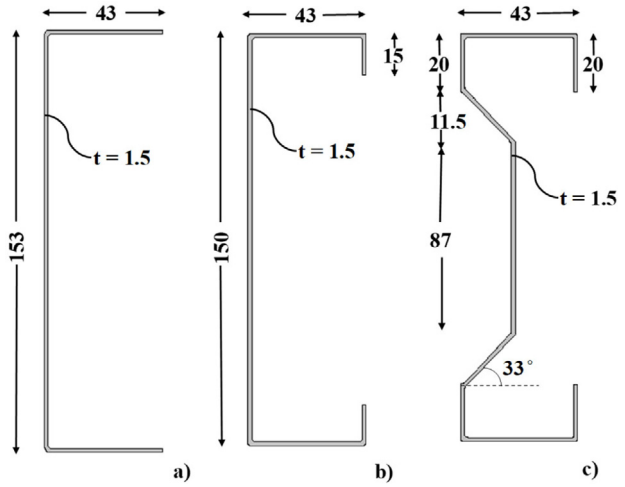

Fig. 1. Geometry of CFS profiles (unit in mm): (a) U-shaped, (b) C-shaped, and (c) Σ-shaped.

as a strengthening solution in critical areas of the buildings. Aiming to further expand the applicability of CFS solutions new synergies must be established combining different structural materials. The versatility of CFS products allows exploring new alternatives, for instance, CF-CFS built-up columns with different geometric shapes using commercially available CFS profiles, which can also be beneficial for retrofitting purposes. The composite solutions are suitable to prevent local buckling phenomena, hence the full capacity of steel can be more effectively exploited, leading to optimal material consumption and spurring, for instance, the use of high-strength cold-formed steel. This type of solution will increase the load-bearing capacity of the CFS columns and the structural fire resistance. Moreover, it is envisaged that this solution shall be used as a prefabricated one (similar to precast concrete elements) and may contribute to allowing the use of LSF in medium-rise buildings.

From the literature review, it was found that there is no research concerning the behavior of concrete-filled cold-formed steel built-up columns. Current design standards such as the EN 1994-1-1 [15] do not consider the use of thin-walled CFS profiles in the design of concrete-filled built-up tubular columns. The behavior of thin-walled cold-formed steel is governed by local buckling phenomena (class 4 cross-sections). Therefore, the applicability of EN 1994-1-1 [15] for the prediction of the buckling resistance of this innovative type of CF-CFS built-up composite columns has been investigated. In this study, 12 CF-CFS built-up specimens including four different cross-section shapes were evaluated. A finite element study using Abaqus [61] was conducted to understand the behavior of the CF-CFS built-up columns before moving forward to the experimental study. The main objective of this research was to investigate the compressive behavior of the presented CF-CFS built-up sections including load-bearing capacity, and buckling modes, understanding the contribution of concrete mitigating local buckling phenomena. The contribution of the CFS built-up sections and concrete infill was evaluated individually to understand the behavior of the composite column and the interaction between steel and concrete. The experimental results were also compared to analytical predictions based on the EN 1994-1-1 [15] considering both the steel gross cross-section area and effective cross-section area determined according to the EN 1993-1-3 [62]. Also, a tailored approach is proposed and verified against the obtained experimental and numerical results.

2. Preliminary design

2.1. Geometry of the CF-CFS built-up sections

In this study, three CFS profiles were used, namely C, U, and Σ-shaped. The individual shapes were arranged to create built-up sections. The geometry details of these sections are showed in Fig. 1. All profiles were fabricated with S280GD + Z structural steel, hot-dip galvanized with zinc on each side (zinc coating of 0.04 mm–275 g/m^2) by cold-forming process.

Fig. 2 also shows the geometry details of the four CF-CFS cross-section shapes tested. These four cross-sections are (a) rectangular built-up cross-section comprising two C-shaped profiles fastened back-to-back and two U-shaped profiles (R-2C + 2U); (b) square built-up cross-section comprising two C-shaped profiles and two U-shaped profiles (S-2C + 2U); (c) rectangular built-up cross-section with two Σ-shaped profiles fastened back-to-back and two U-shaped profiles (R-2Σ + 2U); and (d) square built-up cross-section with two Σ-shaped and two U-shaped profiles (S-2Σ + 2U). All the specimens were filled with lightweight concrete with a density of 1850 kg/m^3. The individual profiles of these sections were connected using self-drilled fasteners with a diameter of 6.3 mm and a length of 45 mm (embedded on lightweight concrete). All specimens have a length of 1050 mm. The considered fastener spacing along the column was 237.5 mm. End distance of 50 mm also has been considered for the first row of fasteners of the CF-CFS built-up column. The location of fasteners is shown in Fig. 2 and the distances of the fasteners are listed in Table 1.

2.2. Mechanical properties

2.2.1. Steel

The mechanical properties of the structural steel S280GD + Z275 (hot-dip galvanized with zinc on each side (zinc coating of 0.04 mm–275 g/m^2) [63] were obtained using a series of tensile coupon tests performed according to ISO 6892-1 [64]. Each test sample was cut in the longitudinal direction of forming from the lipped channel profile. The coupons were manufactured according to the ISO 6892 [64]. The coupon tests were performed using a universal testing machine with 600 kN capacity. The experimental tests were performed according to Method A defined in ISO 6892-1 [64], considering a strain rate control of 0.00007 s^{-1} in range 1 and 0.00025 s^{-1} in range 2.

Mechanical properties such as modulus of elasticity (E_s), yield strength (f_y), ultimate strength (f_u), and proportional stress limit (f_p) were determined. The tensile coupon test samples and dimensions for S280GD + Z and corresponding stress–strain curve are presented in Fig. 3. Also, the mentioned mechanical properties are listed in Table 2. Summarizing the average modulus of elasticity was measured 204 GPa. The average values for proportional stress limit, yield stress (0.2% proof stress), and ultimate stress were 212.5 MPa, 306.81 MPa, and 424.04 MPa, respectively.

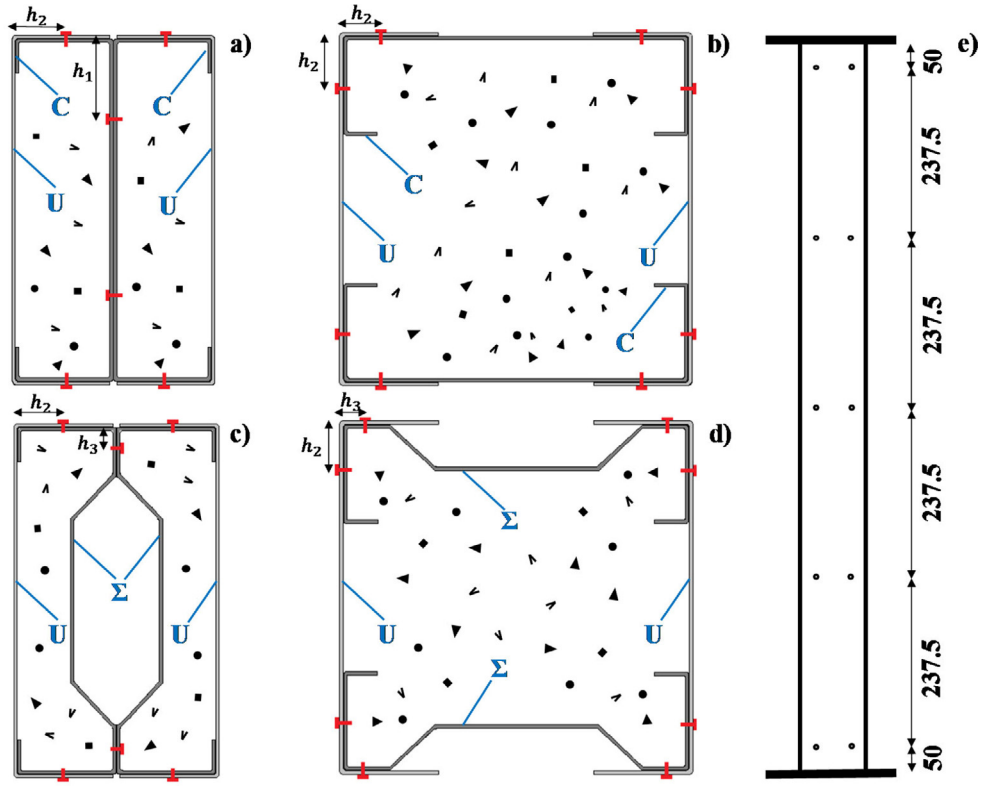

Fig. 2. Built-up cross-sections (unit in mm); (a) R-2C + 2U, (b) S-2C + 2U, (c) R-2Σ + 2U, (d) S-2Σ + 2U, (e) fastener spacing along the length.

Table 2
Mechanical properties of the S280GD + Z275 steel.

Sample	E_s (GPa)	$\overline{E}_s$ (GPa)	f_y (MPa)	$\overline{f}_y$ (MPa)	f_u (MPa)	$\overline{f}_u$ (MPa)	f_p (MPa)	$\overline{f}_p$ (MPa)
#1	205.23		302.54		422.47		208.28	
#2	203.90	204.18	308.92	306.81	426.61	424.04	210.97	212.50
#3	203.42		308.98		423.04		218.24	

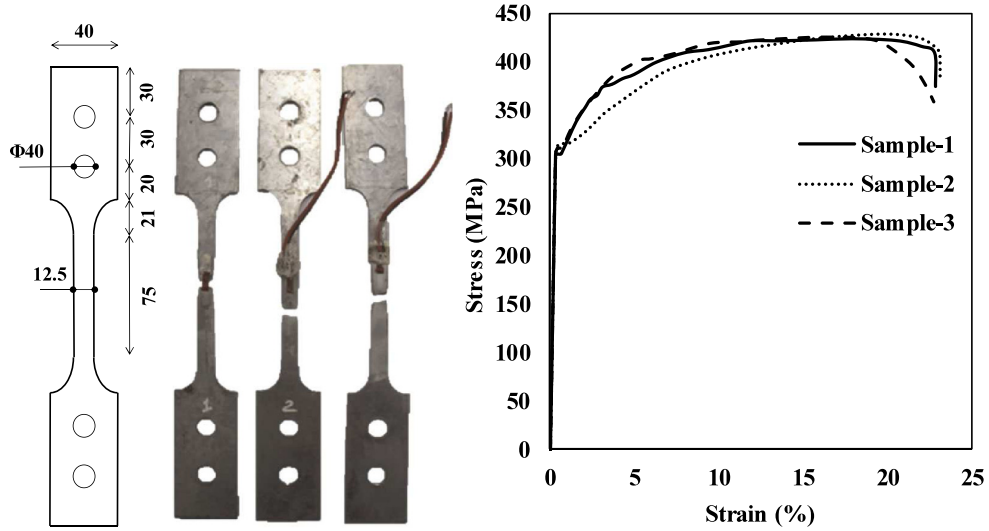

Fig. 3. Tensile coupon test results.

2.2.2. Concrete

The lightweight concrete was used with the mix proportion listed in Table 3. Three standard concrete cubic tests were tested to determine the material properties of concrete. The concrete cubic tests dimensions were 150 mm × 150 mm ×150 mm. The concrete cubic dimensions and test procedures were based on BS EN 206-1:2013 [65] for concrete compression testing (Fig. 4). The average density of the concrete ($\overline{D}$) calculated was 1856 kg/m^3. The compressive cube strength of concrete ($f_{ck,cube}$) for the different tests, was 26.5, 31.2, and 32.8 MPa, respectively. The average value ($\overline{f}_{ck,cube}$) was 30 MPa. Therefore, the mean concrete compressive strength ($\overline{f}_{cm}$) and modulus of elasticity

Table 3
The lightweight concrete mix proportion (kg/m³).

Lightweight aggregate LECA 2–4	Lightweight aggregate LECA 3–8	Sand	Water	Cement CEM I 42.5R	Super plasticizers (Viscocrete-V3000)
294.8	245.6	595.0	204.5	451.5	7.8

($\overline{E}_c$), based on EN 1992-1-1 [66] were taken as 33 MPa and 31.476 GPa, respectively. Table 4 summarizes the measured density, concrete cubic strengths, mean concrete compressive strength, and modulus of elasticity. The mathematical model for the compressive stress–uniaxial strain (σ_c- ε_c) curve of concrete was plotted in Fig. 4-c according to Eqs. (1)–(2).

$$\sigma_c = \frac{(k\eta - \eta^2) f_{cm}}{1 + (k-2)\eta} \tag{1}$$

$$\eta = \frac{\varepsilon_c}{\varepsilon_{c1}} \text{ and } k = 1.05 E_{cm} \frac{\varepsilon_{c1}}{f_{cm}} \tag{2}$$

The strain at peak stress $\varepsilon_{c1} = 0.0021$, was adopted from EN 1992-1-1 [66] for concrete with the same mean compression strength (f_{cm}). However, the expression presented by EN 1992-1-1 [66] is valid just for a strain less than nominal ultimate strain (ε_{cu1}) which is 0.0035 for this concrete. This is not a problem for a standard structural analysis as the strain is usually less than the nominal ultimate strain. In this study as high strain crushing may occur; the extension of the curve was plotted based on Eq. (3) [67] as shown in the red curve of Fig. 4-c. In Eq. (3), α_1, α_2, and α are the factors and suggested to be 0.5, 1, and 20, respectively [67]. Moreover, μ and β_1 are calculated according to Eq. (4).

$$\sigma_c = f_{cm}\left[\frac{1}{\beta_1} - \frac{sin(\mu^{\alpha 1}\alpha_2 \pi/2)}{\beta_1\, sin(\alpha_2 \pi/2)} + \frac{\mu}{\alpha}\right] \tag{3}$$

$$\mu = \frac{\varepsilon_c - \varepsilon_{cu,A}}{\varepsilon_{cu,B} - \varepsilon_{cu,A}} and\ \beta_1 = \frac{f_{cm}}{f_{cu,A}} \tag{4}$$

Note that $f_{cu,A}$ is the compressive strength at point A (Fig. 4-c) that is calculated according to Eq. (1) corresponding to nominal ultimate strain ($\varepsilon_{cu,A} = \varepsilon_{cu1} = 0.0035$). $\varepsilon_{cu,B}$ also was considered 0.02.

The mathematical model for the tensile stress–strain curve of concrete was plotted in Fig. 4-d. The tensile stress–strain curve is defined in elastic and plastic terms. Tensile stress increases linearly along with modulus of elasticity, up to the reach the peak value (f_{ctm}) which is 2.6 MPa based on EN 1992-1-1 [66] for concrete with the same mean compression strength (f_{cm}). After this point, stress is reduced with the sinusoidal manner and at the cracking strain of 0.001, the stress of $0.05\ f_{ctm}$ is achieved.

2.3. Finite element modeling

A finite element modeling was conducted for understanding the behavior of CF-CFS built-up section. Abaqus was used for modeling the innovative CF-CFS built-up composite sections.

2.3.1. Material properties

The mechanical properties of steel were defined as an elastoplastic material. Modulus of elasticity of $E_s = 210$ GPa and Poisson's ratio of $\upsilon = 0.3$ were used to define the elastic behavior of CFS profiles. Moreover, the plastic behavior with isotropic hardening was derived based on the experimental stress–strain curve with yield stress and ultimate stress of 306.81 and 424.04 MPa, respectively (see Fig. 3). The concrete damaged plasticity (CDP) model in Abaqus [61] was used to define the behavior of concrete material. CDP model consists of compressive and tensile behavior, defined separately in terms of plasticity and damage parameters [61–64]. Modulus of elasticity E_c = 31.476 GPa and mean compression cube strength $f_{cm} = 33.0$ MPa were used (see Table 4). The compressive stress–uniaxial strain (σ_c- ε_c) curve was defined based on EN 1992-1-1 [66]. In addition, concrete tensile behavior is defined as the function of tensile stress and cracking strain based on EN 1992-1-1 [66]. Tensile stress increases linearly along with modulus of elasticity, up to the peak value $f_{ctm} = 2.56$ MPa (see Fig. 4-d). The plasticity parameters including flow potential eccentricity, biaxial/uniaxial compressive strength ratio, dilation angle, viscosity parameter, and the ratio of the second stress were defined based on [68,69] as 0.1, 1.16, 30, 0.01, and 0.67, respectively.

2.3.2. Meshing and interactions

S4R shell element, available in Abaqus element library [61] was used for modeling CFS profiles (see Fig. 5). C3D8R solid element was selected to model the concrete infill. Concerning mesh size, a mesh sensitivity analysis was performed to obtain accurate results with reasonable computational times. Different mesh sizes of 5 mm, 10 mm, 15 mm, and 20 mm were analyzed. As the difference between the results from models with a mesh size of 5 mm and 10 mm was negligible (≤1%). Moreover, a 5% difference between the results from models with a mesh size of 10 mm and models with a mesh size of 15 mm were observed. Therefore, a mesh size of 10 mm was considered for CFS profiles and concrete infill. "General contact" was used to define the interaction between steel parts and steel to concrete surfaces. The contact properties among all surfaces were defined including normal hard contact and penalty tangential contact. A friction coefficient sensitivity analysis conducted by Lam et al. [70] and their results reported a negligible effect of friction coefficient value on axial capacity of composite columns. Therefore, a friction coefficient of 0.3 was defined as tangential contact property. The combined "Beam connector and fastener" approach from the Abaqus library was selected to model fasteners. In this technique, the "Beam connector" defined the connection between two nodes of two surfaces. The "fastener" tool applied the real radius of the fasteners to the beam connector from one certain surface to another one. Previous research carried out by the authors showed that the combined "Beam connector and fastener" approach represents the fasteners effects accurately [71]. The modeling technique for the combined "beam connector and fastener" is shown in Fig. 5.

2.3.3. Analysis procedure and boundary condition

Two reference points including RP-1 and RP-2 defined on each column end to apply displacement loading and boundary conditions. Each column end cross-section was coupled to the corresponding reference point. Moreover, the shear deformations at both ends were restrained. The nonlinear dynamic explicit was used to apply pure compression displacement loading to the models. The displacement loading was applied to the models using the "smooth amplitude" technique available in Abaqus [61] to avoid convergence error. The scaling factor (Δt) also was considered for CFS and lightweight concrete to conduct a quasi-static analysis using the dynamic explicit Solver in Abaqus using Eq. (5), where, L^e is the smallest element size and C_d is the wave speed of the material and is calculated according to Eq. (6). Note that the ratio (ALLSD/ALLIE) of the energy dissipated by viscous damping (ALLSD) to the total strain energy (ALLIE) remained below 1%.

$$\Delta t = \frac{L^{el}}{C_d} \tag{5}$$

$$C_d = \sqrt{\frac{E}{\rho}} \tag{6}$$

2.3.4. Initial imperfection and residual stresses

The elastic buckling analysis was carried out to consider geometric imperfections. The pinned support was defined as the boundary condition for the elastic buckling analysis (see Fig. 5). The first buckling mode was selected to be used as input for the imperfections (Fig. 6) [52,53]. Concerning the magnitude of the imperfections, three scenarios were considered based on previous studies including (a) scenario 1

Table 4
Mechanical properties of the tested concrete cube samples.

Test	D (kg/m³)	$\overline{D}$ (kg/m³)	Max. load (kN)	$f_{ck,cube}$ (MPa)	$\overline{f}_{ck,cube}$ (MPa)	$\overline{f}_{cm}$ (MPa)	f_{cd} (MPa)	$\overline{E}_c$ (GPa)	ε_{c1}
#1	1848		596.2	26.5					
#2	1860	1856	702.5	31.2	30	33	25	31.476	0.0021
#3	1860		736.9	32.8					

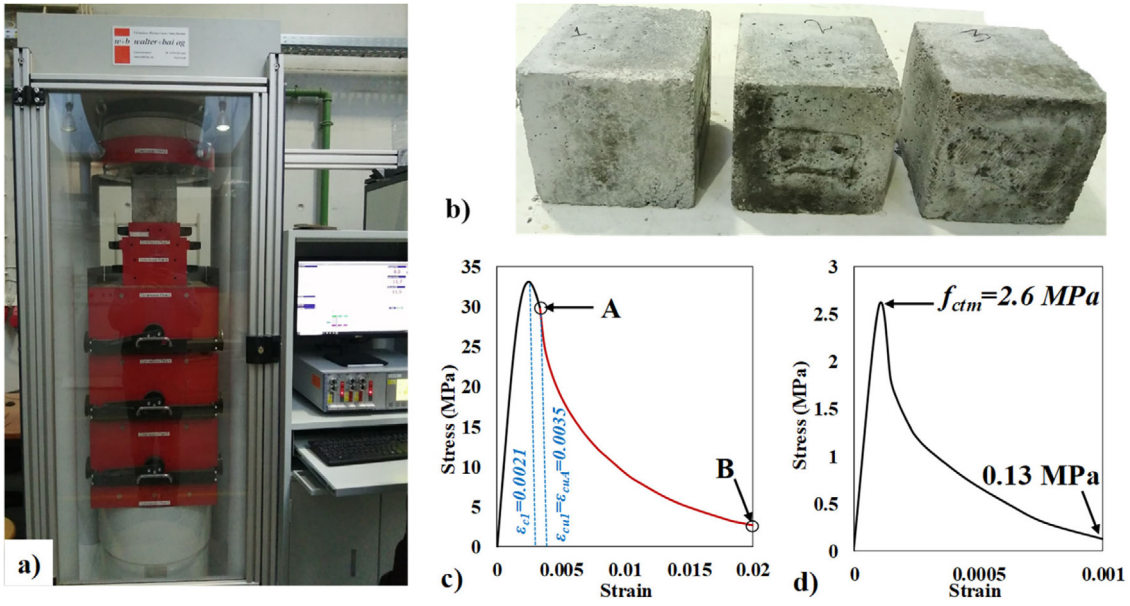

Fig. 4. The standard concrete cube tests and results; (a) compressive test machine, (b) cubic test samples, (c) compressive behavior and (d) tensile behavior.

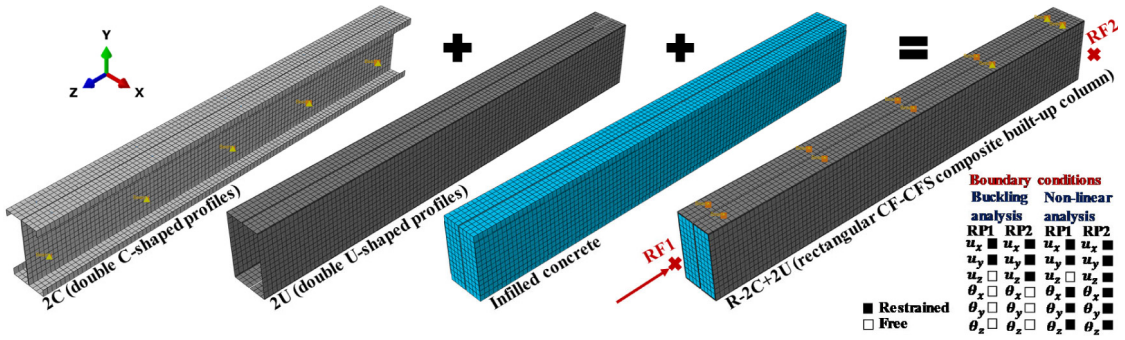

Fig. 5. Meshing and boundary conditions for the FE model.

(S1): no imperfection [58–60], (b) scenario 2 (S2): 1/300 of the column's length based on EN 1994-1-1 [15], and (c) scenario 3 (S3): 1/1000 of the column's length [38,49].

Note that the first predicted buckling mode by Abaqus shows a global buckling mode only for the models R-2C + 2U, S-2C + 2U, and R-2Σ + 2U (Fig. 6). Concerning S-2Σ + 2U model, since linear buckling analysis showed local buckling modes for the first 200 modes, the local buckling mode (see Fig. 6-d) was then used as input for the geometric imperfection in the nonlinear dynamic analysis. The imperfection magnitudes used for local buckling were (a) scenario 1 (S1): no imperfection [58–60], (b) scenario 2 (S2): 1/200 of the section's height [72], and (c) scenario 3 (S3): 1/450 of the section's width [44].

Previous studies [6,7,58–60] reported that residual stresses have a negligible effect on the axial capacity of the composite columns due to support provided to the steel tubes by the concrete. Therefore, residual stresses were not included in the current FE models.

3. Experimental campaign

3.1. Introduction

In this experimental study, 12 specimens including four configurations of CF-CFS built-up columns were tested. The closed built-up CFS specimens were built using C-shaped and U-shaped and Σ-shaped profiles (as presented in Fig. 1 and Table 1). A general view of the experimental tests is shown in Fig. 7 and the general information is listed in Table 5.

3.2. Test set-up and instrumentation

A 5000 kN capacity hydraulic testing machine was used to apply the axial compressive force to the CF-CFS built-up short column specimens. Fig. 8 shows a schematic view of the test set-up. The innovative CF-CFS built-up short columns were positioned in the testing machine, ensuring perfect alignment and verticality of the specimens. Loading was applied under displacement control assuming a constant rate of

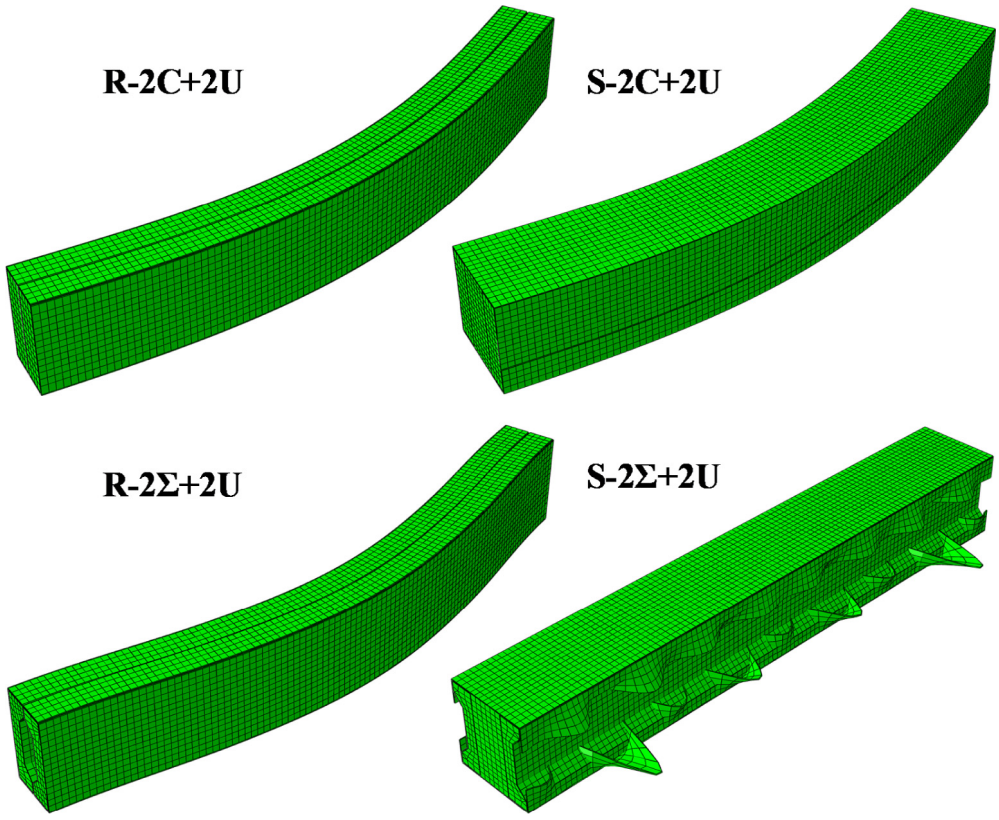

Fig. 6. Buckling modes for the FE models.

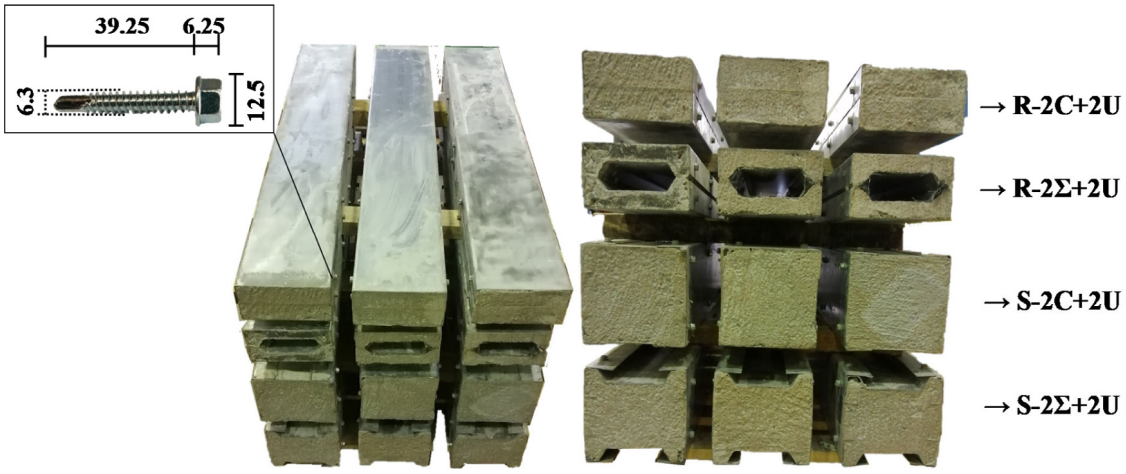

Fig. 7. The experimental specimens (unit in mm).

Table 5
Experimental campaign.

Configurations	Loading	Boundary conditions	Repetitions
R-2C + 2U	Displacement controlled	Fixed supports	3
S-2C + 2U	until failure – 0.01 mm/s		3
R-2Σ + 2U			3
S-2Σ + 2U			3
Total			12

0.01 mm/s. The CF-CFS built-up column tests were stopped when clear drops of axial loads were observed. A 100-mm range Linear Variable Differential Transformer (LVDT) was used to measure the end shortening of the specimens. This LVDT was placed to the bottom bearing plates (LVDT-7) as shown in Fig. 9.

In the first test, a set of two endplates were used at both ends of the short columns, simulating a CFS track channel (S-2 Σ + 2U-1), however, premature local crushing phenomena was observed at the end of the short column (see Fig. 16-d). To prevent this phenomenon a specific device was fabricated to protect both ends of the short columns avoiding localized crushing. The clamping devices were connected to the column ends as shown in Fig. 9. The column ends were also corrected and rectified using cement mortar, ensuring that both ends were parallel and that both concrete and steel profiles were perfectly aligned and leveled.

Six LVDT were positioned along the length of the column in both orthogonal directions to measure out-of-plane deformations (Fig. 10).

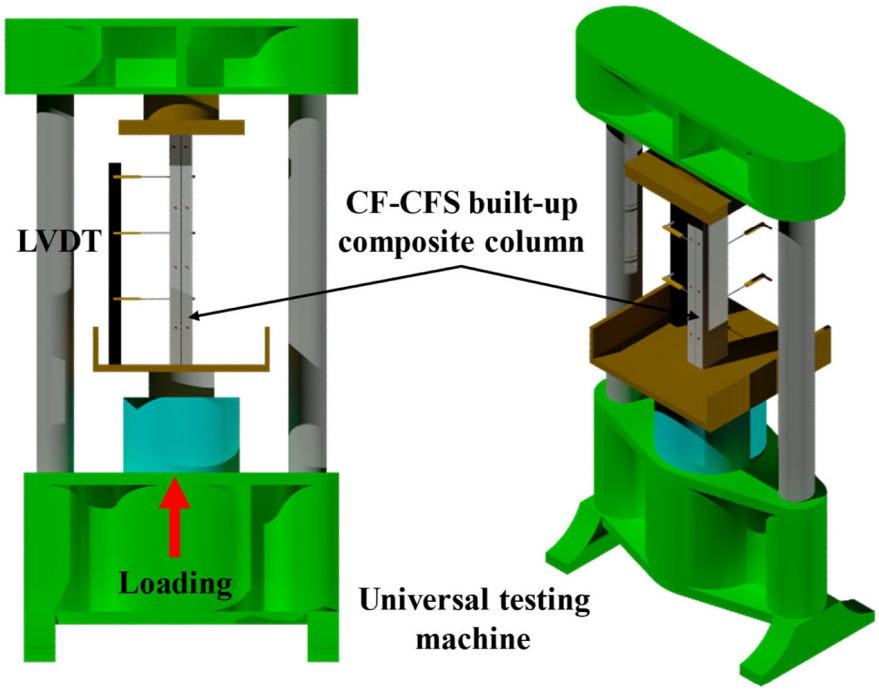

Fig. 8. Schematic view of the setup.

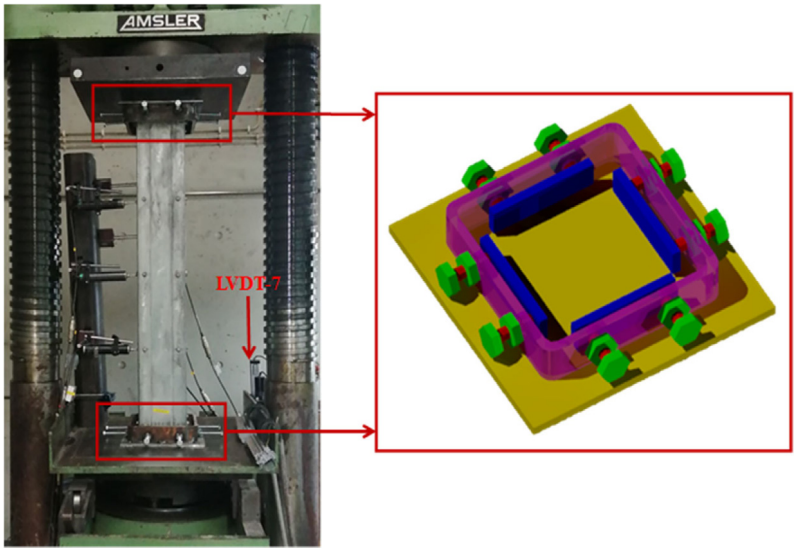

Fig. 9. Experimental test setup and clamping device.

Strain gauges were positioned in the perimeter of the tested cross-sections (the same direction of the loading) at various levels, as depicted in Fig. 11.

4. Results and discussion

4.1. Failure modes

The observed buckling modes for the innovative CF-CFS built-up composite column corresponding to the buckling load are presented in Fig. 12. In Fig. 12-a, showing the deformation of the R-2C + 2U specimen, the distortional and local buckling modes are visible in the external plain channels (U-shaped profiles). Moreover, due to local buckling, a gap between both internal C profiles appeared. From observations, local buckling occurred first on the web of the plain channels (U-shaped profiles) between fasteners. The fastener spacing and position influence the occurrence of distortional and local buckling. Moreover, there were no shear deformations at the fastener locations during the loading of all tested CF-CFS built-up columns. In Fig. 12-b, showing the deformation of the S-2C + 2U specimen, the distortional and local buckling modes are visible in the external plain channels (U-shaped profiles). Fig. 12-c shows the deformed shape of the R-2Σ + 2U specimen. The distortional buckling mode occurred on the flange of the U-shaped profile. Moreover, the local buckling modes are visible in the external plain channels (U-shaped profiles).

Fig. 12-d shows the deformed shape of the S-2Σ + 2U specimen. The distortional buckling mode occurred on the flange of the U-shaped profile. Moreover, the local buckling modes are visible in the web of external plain channels (U-shaped profiles) and internal plain channels (Σ-shaped profiles). From the observation, local buckling at once occurred after distortional buckling for all other types of specimens.

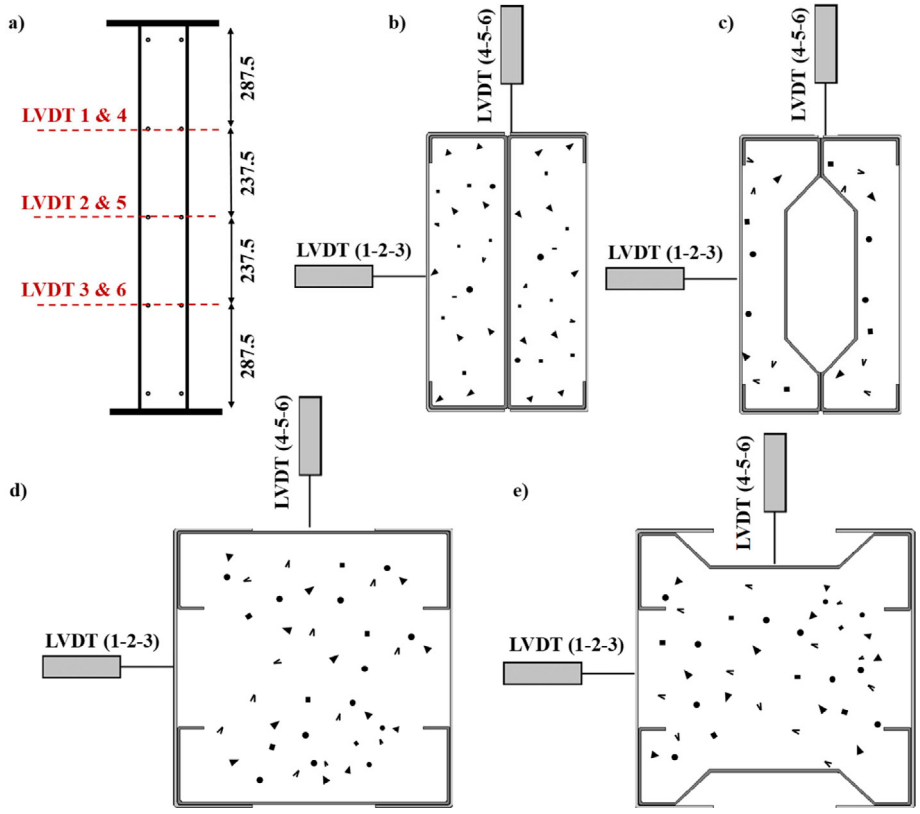

Fig. 10. Positioning of LVDTs for all CF-CFS built-up sections; (a) Positions along the length for the LVDT, (b) R-2C + 2U, (c) R-2Σ + 2U, (d) S-2C + 2U, and (e) S-2Σ + 2U.

Moreover, it is worth mentioning that at the peak load of each one of the tested CF-CFS built-up columns global buckling was not visible.

The final deformed shapes for all the CF-CFS built-up composite columns at the end of the loading stage are presented in Fig. 13.

A comparison between the final deformed shapes of tested specimens and developed FE models is presented in Fig. 14. A close agreement between experimental and FE results was seen in terms of the observed failure modes.

4.2. Load bearing-capacity

The axial load versus end shortening displacement curves for all the innovative CF-CFS built-up columns are plotted in Fig. 15. The numerical results, considering the developed FE models are also plotted and compared with the experimental results. The experimental results showed a good level of reproducibility (<5%). However, for the case of S-2Σ + 2U, a significant difference in terms of load-bearing capacity (20%) was observed between the first test repetition (S-2Σ + 2U-1) and the others (S-2Σ + 2U-2 and S-2Σ + 2U-3). The premature collapse occurred because the clamping devices were not used in the first test. This test result was not considered for additional comparisons.

Comparing the results, it was found that the square CF-CFS built-up columns comprising lipped channels (C) and lipped channels with stiffened web (Σ) (S-2C + 2U and S-2Σ + 2U) provided greater load-bearing capacity, mainly due to the larger concrete area. The results of the experimental tests are also listed in Table 6. The average load-bearing capacity recorded for the tested CF-CFS built-up columns was 704.13 kN (CV = 4.37%), 976.71 kN (CV = 3.79%), 603.64 kN (CV = 3.96%) and 856.96 kN (CV = 1.49%), respectively for the R-2C + 2U, S-2C + 2U, R-2Σ + 2U, and S-2Σ + 2U specimens. The developed finite element models were able to accurately reproduce the observed experimental behavior (Fig. 15). The finite element models slightly underestimated the load-bearing capacity for the R-2C + 2U specimens by 7.3% (656 kN) and for the R-2Σ + 2U specimens by 0.36% (605.83 kN). The finite element models slightly overestimated the load-bearing capacity for the S-2C + 2U specimens by 3.1% (1007 kN) and for the S-2Σ + 2U specimens by 1.8% (873 kN).

Comparing experimental and numerical results with different imperfection magnitudes (scenario 1 to scenario 3), it was found that scenario 2 provided the best fit against experimental results (Table 6). Therefore, the numerical results from scenario-2 were used in Section 5.

The efficiency of the composite action (steel and concrete) may be investigated using the load–weight ratio. Therefore, the load–weight ratios for the concrete–steel section of all tested configurations are listed in Table 7. It can be seen that load–weight ratio (P/W) for the rectangular sections especially the specimens comprising lipped channels with stiffened web (Σ) provided a bigger value.

4.3. Lateral deformation and strain gauge readings

Lateral deformations along the height of the tested columns and in orthogonal directions were measured. In Fig. 16 the monitored deformations along the length of the columns (see Fig. 10) are plotted for two specific load levels, namely $P_{max}/2$ and P_{max}. The results for all specimens show that the deformation of the columns was representing local buckling (global buckling was not observed).

By comparing the results, it was found that the maximum lateral deflection (corresponding load - P_{max}) for rectangular CF-CFS built-up columns (R-2C-2U and R-2Σ + 2U) was recorded in the direction about minor axis (D1). Moreover, the lateral deformation about minor axis (D1) is almost two times higher than those deformations about major axis (D2).

The monitored data from the strain gauges for all the tested configurations are presented in Figs. 17, 18, 19, and 20. The positioning of the strain gauges is depicted in Fig. 11 for all tested configurations. From Figs. 17 to 20, it was observed that during the loading stage the entire cross-section was subjected to compressive stresses. The great majority of the strain gauge readings indicated that when the buckling

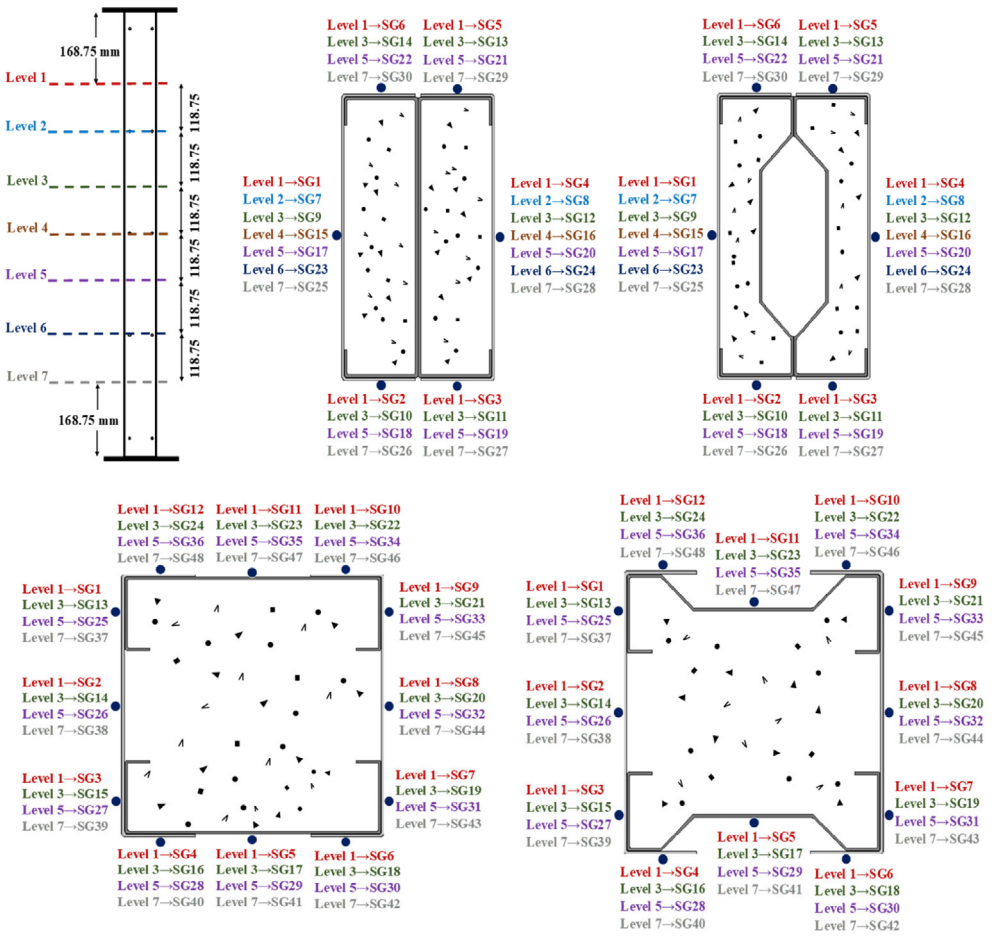

Fig. 11. Positioning of the strain gauges for all configurations.

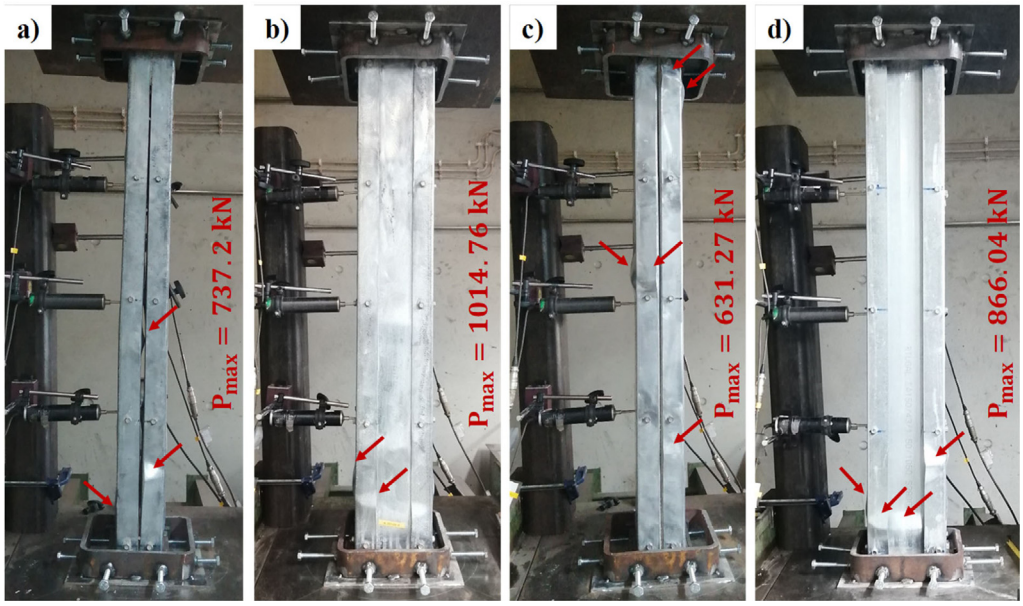

Fig. 12. Deformed shaped of the tested specimens corresponding to the buckling loads; (a) R-2C + 2U, (b) S-2C + 2U, (c) R-2Σ + 2U, and (d) S-2Σ + 2U.

load was reached the limit elastic strain was not attained. However, at some locations, in level-1 (SG-1 and SG2) of the closed built-up R-2C + 2U section, plastic strains were monitored before attaining the buckling load.

This was due to the local buckling and concrete dilatations. Similar behavior was observed from the strain gauges positioned at level 2 of the CFS built-up section S-2C + 2U section (strain gauges positioned in the web of the U-channel; SG13, SG 14, and SG4 from the left-side of the cross-section and SG19, SG20, and SG21 from the right-side

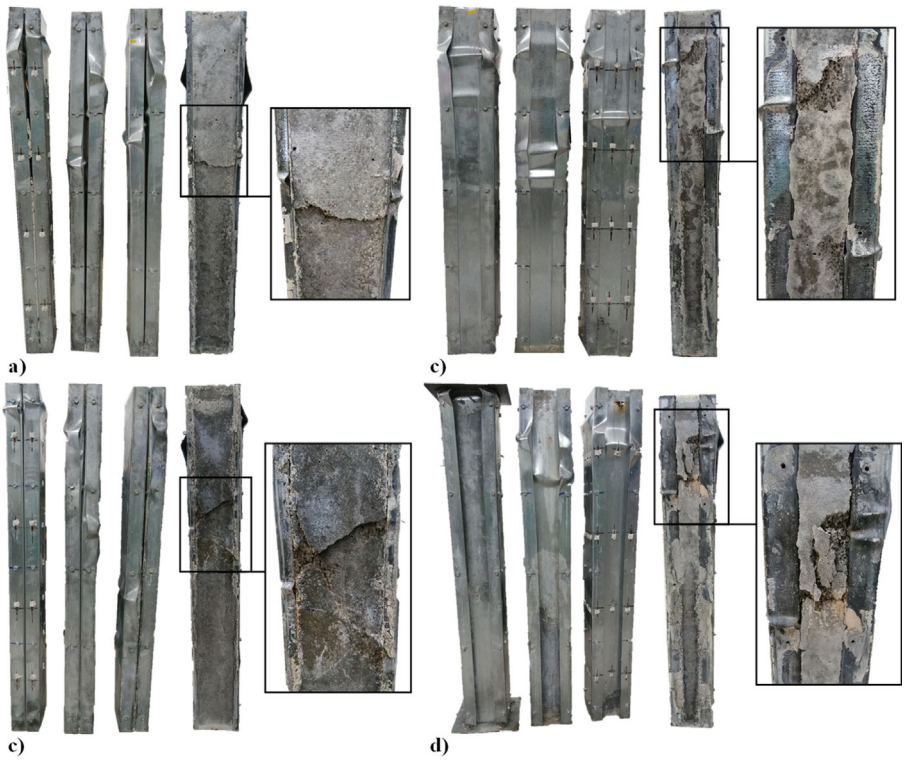

Fig. 13. Final deformed shape of the all specimens; (a) R-2C + 2U, (b) S-2C + 2U, (c) R-2Σ + 2U, and (d) S-2Σ + 2U.

Table 6
Buckling loads recorded in the experimental tests and FE models.

Test Reference	$P_{u,test}$ (kN)	FEM (Scenario-1)		FEM (Scenario-2)		FEM (Scenario-3)	
		P_{FE} (kN)	$\frac{P_{FE}}{P_{u,test}}$	P_{FE} (kN)	$\frac{P_{FE}}{P_{u,test}}$	P_{FE} (kN)	$\frac{P_{FE}}{P_{u,test}}$
R-2C + 2U-1	676.3	753.23	1.11	700.97	1.03	719.33	1.06
R-2C + 2U-2	737.2		1.02		0.95		0.97
R-2C + 2U-3	698.88		1.07		1.00		1.03
Mean value	704.12		1.06		0.99		1.02
Standard deviation	30.78	–	0.04	–	0.04	–	0.04
CV (%)	4.37	–	4.33	–	4.33	–	4.33
S-2C + 2U-1	974.62	1049.69	1.07	1019.05	1.04	1028.03	1.05
S-2C + 2U-2	1014.76		1.03		1.00		1.01
S-2C + 2U-3	940.78		1.11		1.08		1.09
Mean value	976.72		1.07		1.04		1.05
Standard deviation	37.03	–	0.04	–	0.04	–	0.04
CV (%)	3.791	–	3.78	–	3.78	–	3.78
R-2Σ + 2U-1	590.26	622.25	1.05	610.27	1.03	622.1	1.05
R-2Σ + 2U-2	631.27		0.98		0.96		0.98
R-2Σ + 2U-3	589.38		1.05		1.03		1.05
Mean value	603.63		1.03		1.01		1.03
Standard deviation	23.93	–	0.04		0.04	–	0.04
CV (%)	3.96	–	3.88		3.88	–	3.88
S-2Σ + 2U-1*	712.99		1.26		1.20		1.23
S-2Σ + 2U-2	866.04	905.49	1.04	858.24	0.99	882.42	1.02
S-2Σ + 2U-3	847.87		1.06		1.012		1.04
Mean value	856.955		1.05		1.00		1.03
Standard deviation	12.84	–	0.01	–	0.01	–	0.01
CV (%)	1.49	–	1.49	–	1.49	–	1.49
Mean value (all)			**1.05**	–	**1.01**	–	**1.03**
Standard deviation (all)			**0.019**	–	**0.02**	–	**0.012**
CV (%) (all)			**1.8**	–	**2.2**	–	**1.2**

S-2Σ + 2U-1* was not considered in comparison and discussion.

recorded plastic strains). This was due to the fact that local buckling and concrete dilatations occurred close to the location of strain gauges. Also, SG14 shows the highest plastic strain compared to the other strain gauges due to the thinner plate thickness in its location. For the R-2Σ + 2U specimen (Fig. 19), the SG-1 and SG-23 recorded plastic strain and the rest of the other strain gauges behaved only linearly. Also, it was observed that the entire cross-section presented compressive stresses and only SG5 suddenly turned to tensile stress due to the occurrence of

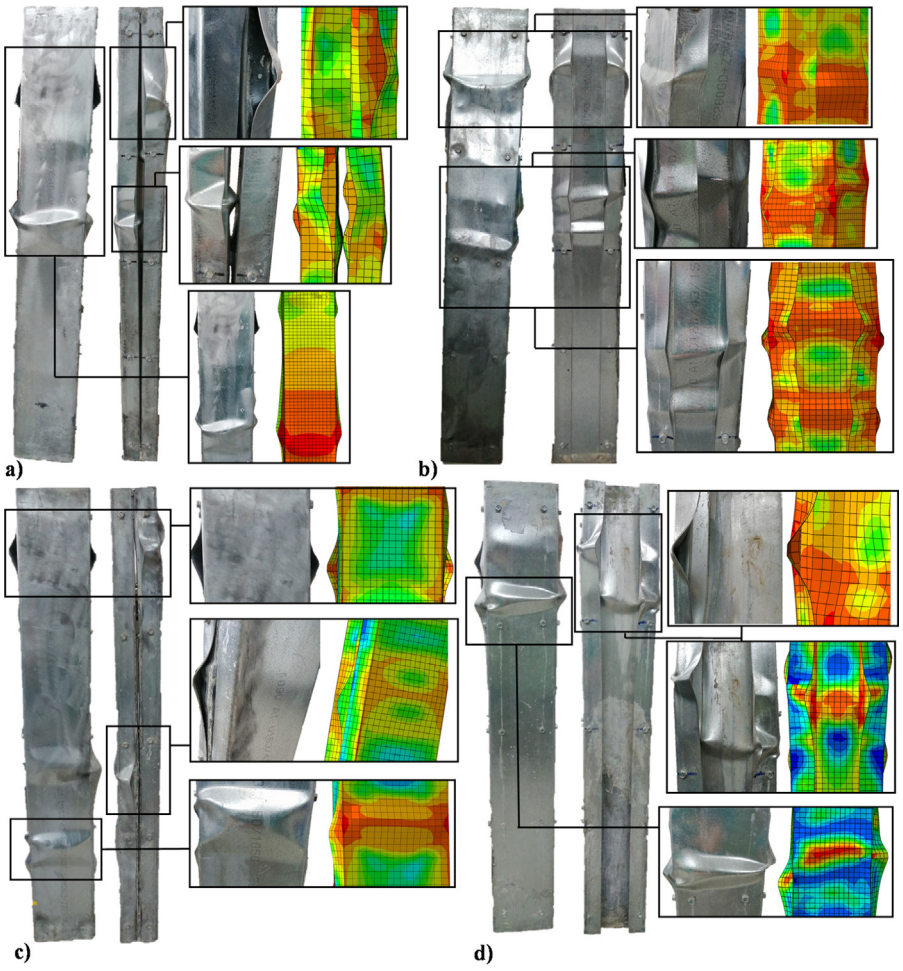

Fig. 14. Final deformed shape for tested specimens and FE model; (a) R-2C + 2U, (b) S-2C + 2U, (c) R-2Σ + 2U, and (d) S-2Σ + 2U.

Table 7
Load–weight ratio for experimental specimens.

Test reference	$P_{test,average}$ (kN)	W_{sum} (N)	P/W_{sum}
R-2C + 2U	704.13	351.0	2005.7
S-2C + 2U	976.71	533.9	1829.1
R-2Σ + 2U	603.64	294.3	2050.6
S-2Σ + 2U	856.96	473.3	1810.3

the distortional buckling mode in the plain channel flange (U-shaped profiles) between fasteners. Fig. 20 shows that during the loading the entire cross-section was subjected to compressive stresses and then four strain gauges from the same side and different levels of the plain channel flange (U-shaped profiles) turned to tensile stresses. Also, it was observed that SG6, SG8, SG20, SG26, SG43, and SG44 suddenly turned to tensile stress due to the buckling occurrence in the web and flange of the plain channel (U-shaped profiles) between fasteners (the distortional buckling mode for SG6 and local buckling mode for the others).

5. The contribution of the individual components of the composite member

In this section, the contribution of individual components, namely CFS sections and concrete infill, on the load-bearing capacity of the composite column was investigated. For this purpose, the axial load bearing capacity for both contributing parts (steel sections and concrete infill) were measured using the results obtained from the validated numerical models.

Additionally, the behavior of the bare CFS closed built-up columns was assessed using the finite element method, to assess in detail the influence of the concrete infill in the overall behavior of the composite solution.

The geometries, boundary conditions, interaction among steel surfaces, and mesh size considered were the same as for the CF-CFS built-up sections to allow the direct comparison of the results. The CFS built-up column models were analyzed using elastic buckling analysis to consider geometric imperfections. Since linear buckling analysis showed local buckling modes for the first 300 modes, the local buckling mode (see Fig. 21) was then used as input for the geometric imperfections in the nonlinear static analysis. The same magnitude for the imperfections (0.765 mm) was considered. Additional details concerning the adopted modeling techniques, mesh sensitivity analysis, and verification of bare CFS columns is available in [71]. It should be noted that the results of the bare CFS closed built-up columns were also verified against experimental data presented in [73].

The finite element load-bearing capacity for CF-CFS built-up composite column (P_{CF-CFS}), concrete infill contribution (P_{CF}), cold-formed steel contribution (P_{CFS}) and CFS built-up columns (P_{CFS_b}) are listed in Table 8. Note that the results of Scenario-2 from Section 4.2 were selected as the most accurate for CF-CFS built-up composite columns (P_{CF-CFS}). This was due to the fact that FE modeling with Scenario-2 predicted the capacity of CF-CFS built-up composite columns in closer agreement (less than 1%) with experimental results. In the composite solution, the contribution of the steel part is higher than the load-bearing capacity of the bare steel cold-formed steel closed built-up columns, clearly showing the advantage of combining steel and concrete and the contribution of the concrete infill to mitigating local buckling phenomena, hence leading to the higher load-bearing capacity of the steel part.

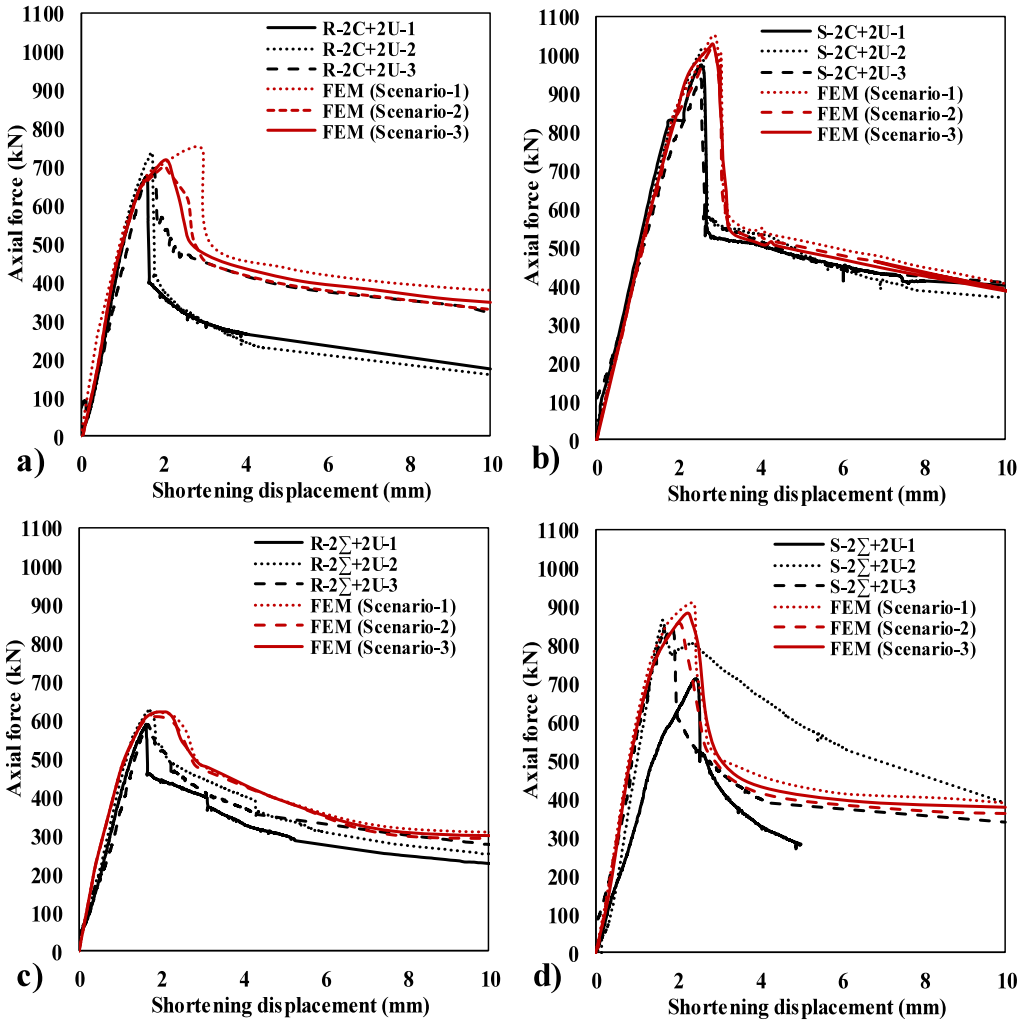

Fig. 15. Force vs. axial shortening curves for all tested CF-CFS built-up composite columns; (a) R-2C + 2U, (b) S-2C + 2U, (c) R-2Σ + 2U, (d) S-2Σ + 2U.

Table 8
Composite component contribution on load-bearing capacity.

Models	CF-CFS column (kN)	Concrete infill (CF) contribution from CF-CFS		Cold-formed steel (CFS) contribution from CF-CFS		Cold-formed steel built-up (CFS_b) column	
		P_{CF} (kN)	P_{CF}/P_{CF-CFS} (%)	P_{CFS} (kN)	P_{CFS}/P_{CF-CFS} (%)	P_{CFS_b} (kN)	P_{CFS}/P_{CFS_b}
R-2C + 2U	700.97	343.12	48.95	357.85	51.01	256.4	1.39
S-2C + 2U	1019.05	672.77	66.02	346.28	33.98	245.2	1.41
R-2Σ + 2U	610.27	244.84	40.12	365.43	59.88	328.8	1.11
S-2Σ + 2U	858.24	499.32	58.18	358.92	41.82	322.6	1.11

Comparing the composite solution with the bare steel one it was found that the load-bearing capacity of the steel part increased 39%, 41%, 11%, and 11%, respectively for the tested cross-section shapes R-2C + 2U, S-2C + 2U, R-2Σ + 2U, and S-2Σ + 2U.

As listed in Table 8, the contribution of steel in the CF-CFS built-up columns was 51.01%, 33.98%, 59.88%, and 41.82% for R-2C + 2U, S-2C + 2U, R-2Σ + 2U, and S-2Σ + 2U, respectively.

6. Comparison with current design predictions according to the EN 1994-1-1

The resistance ($P_{u,test}$) of all CF-CFS built-up specimens was compared to the design predictions according to the EN 1994-1-1 [15] as listed in Table 9. In general, the plastic resistance ($P_{pl,Rd}$) of the concrete-filled steel tubular columns should be predicted using equation (6.30) of the EN 1994-1-1 [15] (Eq. (7) in this paper). In this equation, the plastic resistance ($N_{pl,Rd}$) of the composite column is predicted by adding the plastic resistance of the steel tubular section, concrete infill, and steel reinforcement. In this case, as no reinforcement was used, the plastic resistance ($N_{pl,Rd,1}$) of the CF-CFS built-up composite sections can be predicted by Eq. (8):

$$N_{\text{pl, Rd}} = A_a f_{yd} + 0.85\, A_c f_{cd} + A_s f_{sd} \tag{7}$$

$$N_{\text{pl, Rd,1}} = A_a f_{yd} + 0.85\, A_c f_{cd} \tag{8}$$

According to the EN 1994-1-1 [15] the 0.85 factor for concrete is used to consider the influence of long-term effect due to acting loads, excluding creep and shrinkage (Eq. (7)). However, this factor can be replaced by 1.0 for concrete-filled tubular sections due to confinement. Therefore, the plastic resistance ($N_{pl,Rd,2}$) of the CF-CFS built-up composite columns were also predicted by Eq. (9):

$$N_{\text{pl,Rd,2}} = A_a f_{yd} + A_c f_{cd} \tag{9}$$

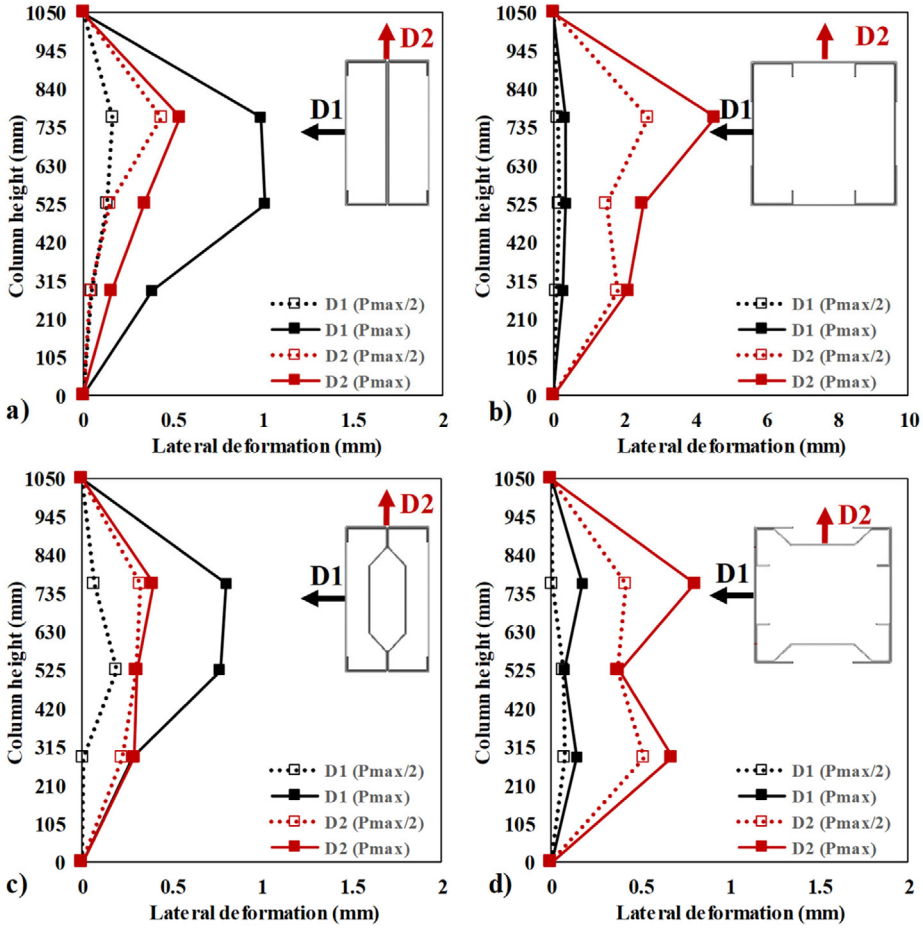

Fig. 16. Lateral displacement based on LVDT records; (a) R-2C + 2U, (b) S-2C + 2U, (c) R-2Σ + 2U, (d) S-2Σ + 2U.

Table 9
Comparison of test results and analytical prediction.

Test reference	A_c (mm^2)	$\bar{\lambda}$	EI_{eff} (kN m^2)	$P_{u,test}$ (kN)	A_a (mm^2)	$N_{b,Rd,1}$ (kN)	$P_{u,test}/N_{b,Rd,1}$	$N_{b,Rd,2}$ (kN)	$P_{u,test}/N_{b,Rd,2}$	A_{eff} (mm^2)	$N_{b,Rd,3}$ (kN)	$P_{u,test}/N_{b,Rd,3}$	$N_{b,Rd,4}$ (kN)	$P_{u,test}/N_{b,Rd,4}$
R-2C + 2U-1				676.3			0.948		0.891			1.319		1.212
R-2C + 2U-2	12 121.50	0.24	354.9	737.2	1485	713.19	1.033	758.65	0.972	830.96	512.53	1.438	557.98	1.321
R-2C + 2U-3				698.88			0.978		0.921			1.363		1.252
Mean value				**704.13**	–	–	**0.987**	–	**0.928**	–	–	**1.373**	–	**1.261**
Standard deviation				**30.79**	–	–	**0.043**	–	**0.040**	–	–	**0.060**	–	**0.055**
CV (%)				**4.37**	–	–	**4.372**	–	**4.372**	–	–	**4.372**	–	**4.372**
S-2C + 2U-1				974.62			1.062		0.976			1.360		1.221
S-2C + 2U-2	21 720.00	0.12	1664.0	1014.76	1485	917.16	1.106	998.61	1.016	830.96	716.5	1.416	797.95	1.271
S-2C + 2U-3				940.78			1.025		0.942			1.313		1.179
Mean value				**976.71**	–	–	**1.064**	–	**0.978**	–	–	**1.363**	–	**1.224**
Standard deviation				**37.02**	–	–	**0.040**	–	**0.037**	–	–	**0.051**	–	**0.046**
CV (%)				**3.79**	–	–	**3.791**	–	**3.791**	–	–	**3.791**	–	**3.791**
R-2Σ + 2U-1				590.26			0.891		0.849			1.101		1.037
R-2Σ + 2U-2	8912.80	0.21	407	631.27	1540	661.88	0.953	695.31	0.907	1128.84	535.74	1.178	569.16	1.109
R-2Σ + 2U-3				589.38			0.890		0.847			1.100		1.035
Mean value				**603.64**	–	–	**0.912**	–	**0.868**	–	–	**1.126**	–	**1.060**
Standard deviation				**23.93**	–	–	**0.036**	–	**0.034**	–	–	**0.044**	–	**0.042**
CV (%)				**3.79**	–	–	**3.965**	–	**3.965**	–	–	**3.965**	–	**3.965**
S-2Σ + 2U-2	18 307.10	0.13	1320	866.04	1540	851.61	1.005	930.17	0.931	1128.84	735.37	1.177	804.02	1.077
S-2Σ + 2U-3				847.87			0.984		0.911			1.153		1.054
Mean value				**856**	–	–	**0.994**	–	**0.921**	–	–	**1.165**	–	**1.065**
Standard deviation				**12.84**	–	–	**0.015**	–	**0.013**	–	–	**0.017**	–	**0.015**
CV (%)				**1.49**	–	–	**1.499**	–	**1.499**	–	–	**1.499**	–	**1.499**
Mean value (all)				–	–	–	**0.989**	–	**0.924**	–	–	**1.265**	–	**1.161**
Standard deviation (all)				–	–	–	**0.067**	–	**0.051**	–	–	**0.125**	–	**0.102**
CV (%) (all)				–	–	–	**6.779**	–	**5.601**	–	–	**9.948**	–	**8.827**
Reliability Index, b				–	–	–	**2.6**	–	**2.2**	–	–	**4.04**	–	**3.54**

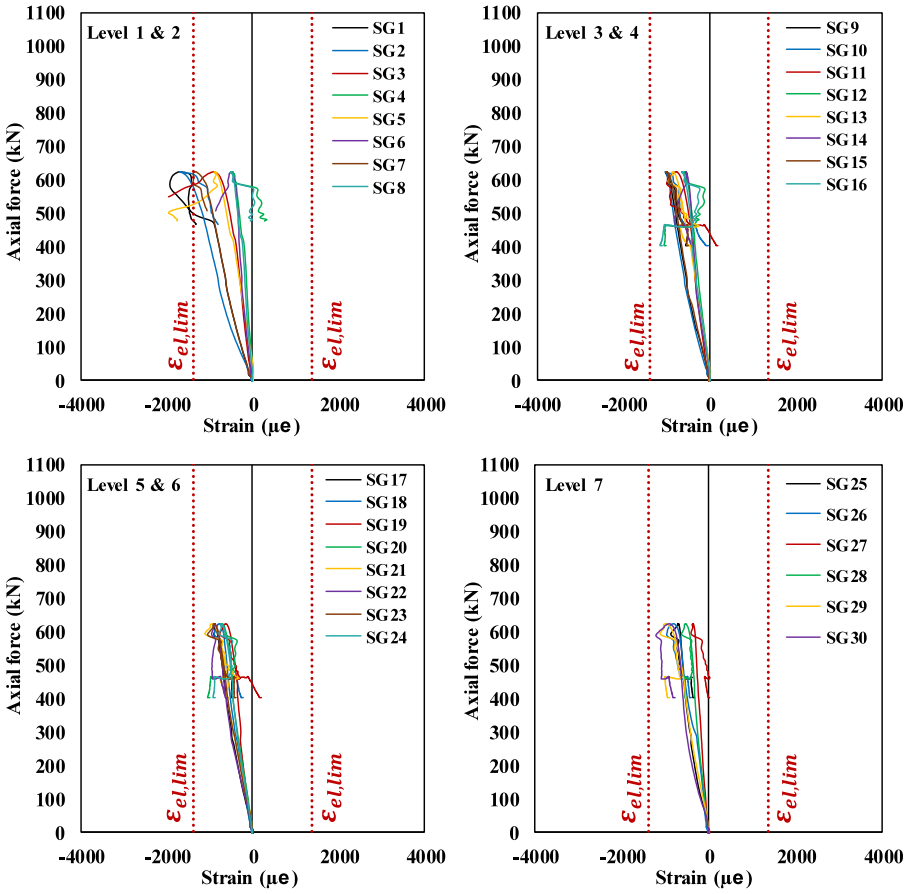

Fig. 17. Force vs. strain curves for R-2C + 2U.

Based on EN 1994-1-1 [15] the effective flexural stiffness (EI_{eff}), steel contribution ratio (δ) and relative slenderness ($\bar{\lambda}$) should be considered as well. The steel contribution ratio (δ) is defined using Eq. (10):

$$\delta = \frac{A_a f_{yd}}{N_{Pl,\ Rd}} \tag{10}$$

According to EN 1994-1-1 [15], a section with $0.2 \leq \delta \leq 0.9$ can be calculated as a composite column. It should be mentioned that all specimens in this study fulfill this requirement. The relative slenderness ($\bar{\lambda}$) for the plane of bending is calculated by Eq. (11), where $N_{pl,Rk}$ is the characteristic value of the plastic resistance. Moreover, N_{cr} for a column with fixed ends is calculated from Eq. (12) where L_e is 0.5×1050 mm, and the effective flexural stiffness (EI_{eff}) is presented as Eq. (13). In Eq. (13), I_a, I_s and I_c are the second moments of area of the structural steel section, the uncracked concrete section, and the reinforcement, respectively, for the bending plane being considered. Moreover, k_e is a correction factor that should be taken as 0.6 according to EN 1994-1-1 [15]. The influence of long-term effects on the effective elastic flexural stiffness must be considered according to (Eq. (14)). The modulus of elasticity of concrete E_{cm} should be reduced to the value $E_{c,eff}$ according to Eq. (15), where φ_t is the creep coefficient that is considered as 1.05 [15]. To calculate the design buckling resistance ($N_{b,Rd}$), the reduction factor must be calculated, based on EN 1993-1-1 [74] Section 6.3.1.2 as presented in Eqs. (16) and (17), where the imperfection factor (α) is defined referring to Table 6.1 of EN 1993-1-1 (in this study curve *b*) [74].

Considering the gross area of the CFS built-up section, the design buckling load (Nb,Rd) is determined using Eqs. (18) and (19).

$$\bar{\lambda} = \sqrt{\frac{N_{pl,Rk}}{N_{cr}}} \tag{11}$$

$$N_{cr} = \frac{\pi^2 (EI)_{eff}}{{L_e}^2} = \frac{\pi^2 (EI)_{eff}}{(0.5L)^2} \tag{12}$$

$$EI_{eff} = E_a I_a + E_s I_s + k_e E_{cm} I_c \tag{13}$$

$$EI_{eff} = E_a I_a + E_s I_s + k_e E_{c,eff} I_c \tag{14}$$

$$EI_{c,eff} = E_{cm} \frac{1}{1 + \left(\frac{N_{G,\ Ed}}{N_{Ed}}\right) \varphi_t} \tag{15}$$

$$\chi = \frac{1}{\Phi + \sqrt{\Phi^2 - \bar{\lambda}^2}} \tag{16}$$

$$\Phi = 0.5 \left[1 + \alpha \left(\bar{\lambda} - 0.2\right) + \bar{\lambda}^2\right] \tag{17}$$

$$N_{\mathrm{b,\ Rd,1}} = \chi N_{\mathrm{pl,\ Rd,1}} \tag{18}$$

$$N_{\mathrm{b,\ Rd,2}} = \chi N_{\mathrm{pl,\ Rd,2}} \tag{19}$$

Moreover, the individual CFS sections used in this study were classified as Class 4 cross-sections based on EN 1993-1-1 [74]. In addition, based on 6.7.1. 8(P) - EN 1994-1-1 [15] the influence of local buckling of the steel section on the resistance shall be considered in the design. Therefore, considering the Effective Width Method detailed in the EN 1993-1-3 [62], the effective areas of the Class 4 cross-sections were determined. Therefore, two other predictions ($N_{\mathrm{b,Rd,3}}$ and $N_{\mathrm{b,Rd,4}}$) can be based on Eqs. (20) and (21).

$$N_{\mathrm{b,Rd,3}} = \chi(A_{eff} f_{yd} + 0.85\, A_c f_{cd}) \tag{20}$$

$$N_{\mathrm{b,Rd,4}} = \chi(A_{eff} f_{yd} + A_c f_{cd}) \tag{21}$$

The effective area of a steel plate element (A_{eff}) is determined according to the EN 1993-1-3 [62] by considering the EN 1993-1-5 (Clause 4.4, and Tables 4.1 and 4.2) [75]. The effective area of a lipped channel was calculated using Eq. (22), where the effective plate length (b_{eff})

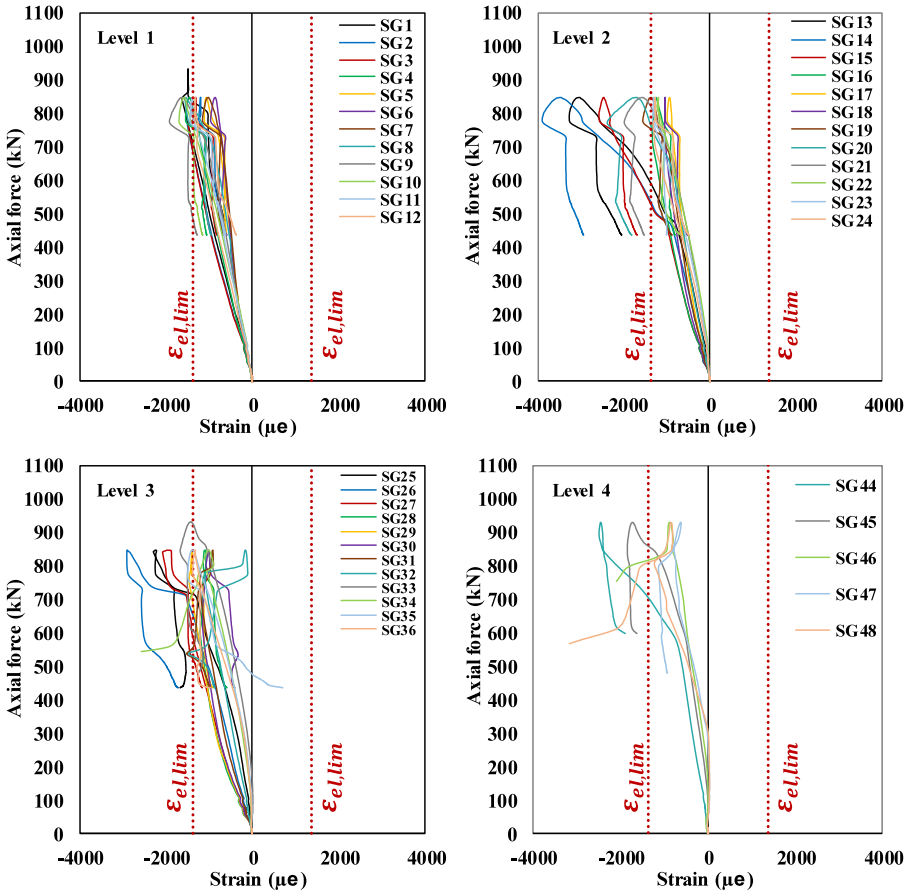

Fig. 18. Force vs. strain curves for S-2C + 2U.

(Eq. (23)) is obtained by calculating the reduction factor for plate buckling (ρ), based both on the elastic local buckling stress (Eq. (24)) and on the elastic distortional buckling stress (Eq. (25)).

$$A_{eff} = t\left[h_{e1} + h_{e2} + 2b_{e1} + 2\left(b_{e2} + c_{e2}\right)c_d\right] \tag{22}$$

$$b_{eff} = \rho.b \tag{23}$$

$$\sigma_{cr} = \frac{k_\sigma \pi^2 E}{12\left(1-\upsilon^2\right)(b/t)^2} \tag{24}$$

$$\sigma_{cr,s} = \frac{2\sqrt{KEI_s}}{A_s} \tag{25}$$

The experimental axial capacities obtained from the experimental tests on the innovative CF-CFS built-up short columns were compared with those buckling design load predictions using the EN 1994-1-1 [15] as given in Table 9. It can be noticed from Table 9 that there is a slight difference (6.5%) between the predicted values based on Eqs. (18) and (19) ($N_{b,Rd,1}$ and $N_{b,Rd,2}$) in the case of concrete-filled cold-formed steel (CF-CFS) built-up short columns. Moreover, there is 9% difference between the predicted values based on Eqs. (20) and (21) ($N_{b,Rd,3}$ and $N_{b,Rd,4}$). But still the predicted values ($N_{b,Rd,1}$), based on the EN 1994-1-1 [15] considering the steel gross cross-section area and the 0.85 coefficient for concrete, are in good agreement with the test results for S-2C + 2U (6.4%) and S-2Σ + 2U (0.6%). The predicted values based on EN 1994-1-1 [15] considering the steel gross cross-section area and the 1.0 coefficient for concrete ($N_{b,Rd,2}$), show slightly unconservative results (8% higher than P_{test}). On the other hand, the predicted value based on EWM [62] for CFS section and the 1.0 coefficient for concrete ($N_{b,Rd,4}$) present close and conservative results (6.5% lower than P_{test}). Moreover, the predicted value based on EWM [62] for CFS section and the 0.85 coefficient for concrete ($N_{b,Rd,3}$) presents a conservative result (the design buckling load for R-2C + 2U, S-2C + 2U, R-2Σ + 2U, and S-2Σ + 2U is 37.3%, 36.3%, 12.6%, and 16.5% lower than P_{test}, respectively). Similarly, the predicted value based on EWM [62] for CFS section and the 1.0 coefficient for concrete ($N_{b,Rd,4}$) also presents a conservative result (the design buckling loads for R-2C + 2U, S-2C + 2U, R-2Σ + 2U, and S-2Σ + 2U are 26.1%, 22.4%, 6%, and 6.5% lower than P_{test}, respectively).

Table 10
Comparison of the concrete-filled contribution for Eurocode predictions and FE results.

Test reference	P_{CF} (kN)	$P_{c1} = 0.85 \times A_c \times f_{cd}$ (kN)	P_{CF}/P_{c1}	$P_{c2} = A_c \times f_{cd}$ (kN)	P_{CF}/P_{c2}
R-2C + 2U	343.12	257.58	1.33	303.03	1.13
S-2C + 2U	672.77	461.55	1.45	543.00	1.23
R-2Σ + 2U	244.84	189.39	1.29	222.82	1.1
S-2Σ + 2U	499.32	389.02	1.28	457.67	1.09
Mean value			**1.34**	–	**1.14**
Standard deviation			**0.08**	–	**0.068**
CV (%)			**5.98**	–	**5.98**

A comparison between finite element model results and EN 1994-1-1 [15] predictions was presented for steel and concrete contributions to understanding and analyzing the validity of the EN 1994-1-1 [15] formulations. The analysis of composite column components was reported in Section 5. To assess the contribution of the concrete infill according to the Eurocode formulation both 0.85 and 1 coefficients (coefficient for concrete considering the influence of long-time acting loads, excluding creep and shrinkage) were considered. As recommended by the Eurocode, adopting the coefficient as 1 provides a better agreement with the FE results (Table 10).

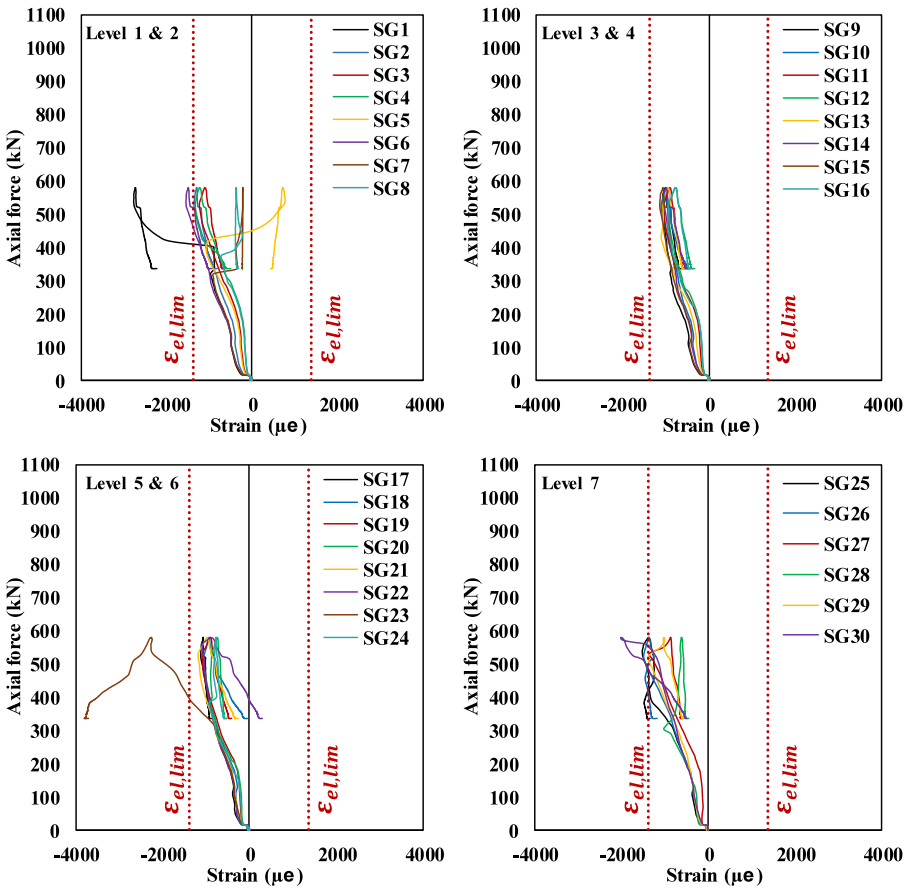

Fig. 19. Figure 19 Force vs. strain curves for R-2Σ + 2U.

For the contribution of the steel component based on the Eurocode, two expressions from Eq. (8) ($A_a \times f_{yd}$) and Eq. (20) ($A_{eff} \times f_{yd}$) were used (see Table 11). As it is indicated, the Eurocode formulation based on the gross sectional area (A_a) overestimated the steel contribution by 23% when comparing with the FE results. This is due to the fact that in prediction based on gross sectional area (A_a), no local buckling effect is considered. When the effective sectional area (A_{eff}) was considered, the Eurocode formulation underestimated by 21% the steel contribution when comparing with the FE results. This difference is due to the lack of specific design guidelines for built-up cold-formed steel sections, since no indication is provided regarding the influence of overlapping steel plates and the restraint provided by the fasteners mitigating local buckling phenomena.

Therefore, a new modification was proposed to determine more accurately the effective area considering the overlapping effect of the steel plates and the confinement provided by the concrete infill. The proposed prediction was obtained based on Eq. (26):

$$N_{\mathrm{b,Rd,5}} = \chi(A_{eff,p} f_{yd} + A_c f_{cd}) \tag{26}$$

where the proposed effective area of a steel plate element ($A_{eff,p}$) is determined according to the EN 1993-1-3 [62] by considering the following assumptions:

- The effective areas of the flanges of U, C, and Σ-shaped profiles were calculated assuming their total thickness (i.e., 3 mm instead of 1.5 mm) as the steel plates were overlapped and fastened to each other, for the R-2C + 2U, S-2C + 2U, and R-2Σ + 2U columns.
- The gross area was considered for concrete-encased steel plates (i.e., webs of the C profiles for the R-2C + 2U columns).
- The effective areas of the webs of U-shaped profiles were calculated assuming their plate width equal to the distance between the fasteners (i.e., 110 mm instead of 153 mm), for the S-2C + 2U and S-2Σ + 2U (square) columns.

The buckling design load predictions using the proposed modification and concrete coefficient 1.0 ($N_{\mathrm{b,Rd,5}}$) were compared with those results obtained from the experimental tests on the innovative CF-CFS built-up short columns as given in Table 12. It can be noticed that there is a close agreement between the predicted values based on proposed modification ($N_{\mathrm{b,Rd,5}}$) and experimental results for all configurations with an average difference of 5% ($P_{u,test}/N_{b,Rd,5}$ = 1.05). The average ratios of $P_{u,test}/N_{b,Rd,5}$ for R-2C + 2U, S-2C + 2U, R-2Σ + 2U, and S-2Σ + 2U were obtained as 1.056, 1.124, 1.001, and 1.019, respectively. A comparison of the analytical predictions based on EN 1994-1-1 [15] and experimental results are plotted in Fig. 22.

Reliability analysis was performed to evaluate the reliability of the predicted methods for CF-CFS built-up short columns. The safety of the design prediction can be relatively evaluated by the reliability index (β). A higher value of the reliability index represents a more reliable design prediction. In this study, the reliability analysis was performed according to the commentaries of the AISC Specification [76] and the NAS Specification [77] with the statistical parameter assumptions based on [52]. More details about reliability analysis are presented in the commentaries of the AISC Specification [76] and the NAS Specification [77].

The reliability index of 4.04 and 3.54 was obtained for the predicted results considering the effective sectional area for CFS built-up elements (Table 9). Smaller values of 2.6 and 2.2 were obtained for those predictions based on EN 1994-1-1 considering the gross cross-sectional area for CFS built-up elements (Table 9). Moreover, a reliability index value of 3 (Table 12) was obtained for the proposed design approach. Hence, considering the effective sectional area provided more reliable predictions for the investigated configurations.

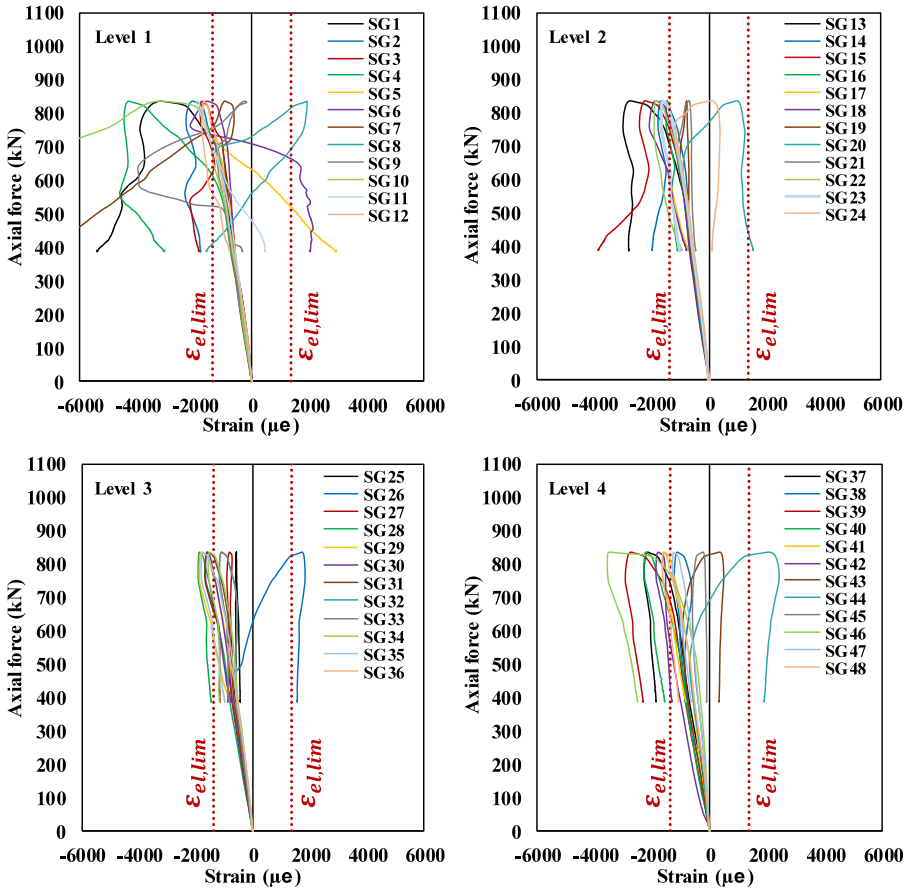

Fig. 20. Force vs. strain curves for S-2Σ + 2U.

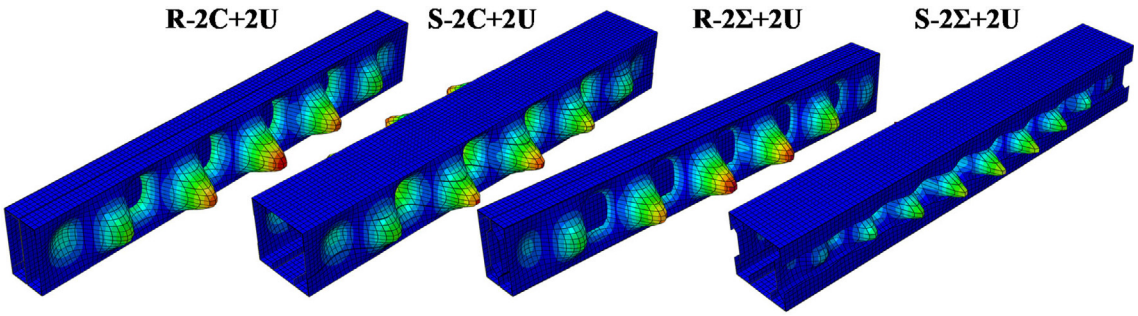

Fig. 21. Buckling modes for CFS built-up columns.

Table 11
Comparison of the CFS built-up sections contribution for Eurocode predictions and FE results.

Test reference	P_{CFS} (kN)	$P_{s,\,a}$ = $A_a \times f_{yd}$ (kN)	$P_{CFS}/P_{s,a}$	$P_{s,\,eff}$ = $A_{eff} \times f_{yd}$ (kN)	$P_{CF}/P_{s,eff}$
R-2C + 2U	357.85	455.61	0.78	254.94	1.40
S-2C + 2U	346.28	455.61	0.76	254.94	1.35
R-2Σ + 2U	365.43	472.48	0.77	346.34	1.05
S-2Σ + 2U	358.92	472.48	0.76	345.34	1.04
Mean value			**0.77**	–	**1.21**
Standard deviation			**0.01**	–	**0.19**
CV (%)			**1.60**	–	**15.95**

7. Conclusions and future work

In this paper, an experimental investigation on concrete-filled cold-formed steel (CF-CFS) built-up short columns, comprising four different cross-section shapes, was presented. A numerical investigation also was performed to obtain the contribution of individual components including steel sections and concrete-filled on the composite column axial capacity, based on validated numerical models. The findings are summarized as follows:

1. The average buckling loads for R-2C + 2U, S-2C + 2U, R-2Σ + 2U, and S-2Σ + 2U composite columns were 704.13 kN, 976.71 kN, 603.64 kN, and 856.96 kN, respectively. The square section columns showed a higher load-bearing capacity comparing to the rectangular ones due to the larger concrete area. In terms

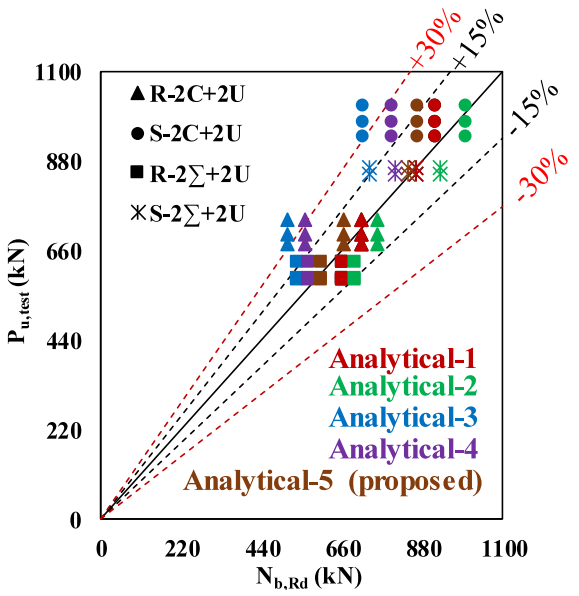

Fig. 22. Comparison of test results and analytical predictions.

Table 12
Comparison of test results and proposed analytical prediction.

Test Reference	$A_{eff,p}$ (mm^2)	$N_{b,Rd,5}$ (kN)	$P_{u,test}$ (kN)	$P_{u,test}/N_{b,Rd,5}$
R-2C + 2U-1			676.3	1.014
R-2C + 2U-2	1184.14	666.34	737.2	1.106
R-2C + 2U-3			698.88	1.048
Mean value				**1.056**
Standard deviation				**0.046**
CV (%)				**4.372**
S-2C + 2U-1			974.62	1.121
S-2C + 2U-2	1179.47	904.87	1014.76	1.168
S-2C + 2U-3			940.78	1.082
Mean value				**1.124**
Standard deviation				**0.042**
CV (%)				**3.791**
R-2Σ + 2U-1			590.26	0.978
R-2Σ + 2U-2	1239.11	602.99	631.27	1.046
R-2Σ + 2U-3			589.38	0.977
Mean value				**1.001**
Standard deviation				**0.039**
CV (%)				**3.965**
S-2Σ + 2U-2	1360.82	873.36	866.04	1.029
S-2Σ + 2U-3			847.87	1.008
Mean value				**1.019**
Standard deviation				**0.015**
CV (%)				**1.499**
Mean value				**1.060**
Standard deviation (all)				**0.014**
CV (%) (all)				**1.336**
Reliability index, b				**3.0**

of strength-to-weight ratio, the highest value was obtained for R-2Σ + 2U columns (2050.6), followed by R-2C + 2U (2005.7), S-2C + 2U (1829.14), and S-2Σ + 2U (1810.3). Perhaps due to the high confinement effect of concrete in rectangular columns.

2. The local buckling in the plain channels was observed as the predominant buckling mode for all CF-CFS built-up short columns. However, for the case of S-2Σ + 2U, the distortional buckling on the flanges of the plain channels governed the failure mode.
3. The results showed that the load bearing capacity of CFS built-up sections when were used in CF-CFS column increased compared to those CFS built-up with no concrete since concrete enhanced built-up steel sections against buckling deformation.
4. The comparison between finite element results and code predictions was shown that the EN 1994-1-1 [15] formulations based on the gross sectional area (A_a) overpredicted the steel contribution, however, the effective cross-sectional area (A_{eff}) in the Eurocode formulations estimated significantly lower contribution.
5. A modification was proposed by considering overlapping plates and fastener positioning to reduce the slenderness of the individual plate elements. Moreover, the area of the fully encased plate elements was considered fully effective due to the confinement provided by the concrete infill. This resulted in a close agreement between the predicted values and experimental results. It should be mentioned that at this stage the proposed methodology is only valid for the tested configurations. Additional studies are required to fully validate the adopted assumptions and to generalize the adopted formulation for any type of Class 4 cross-section shape.
6. A close agreement between the results obtained using experimental tests and FE models in terms of deformation and load bearing capacity was observed. Therefore, these used techniques for finite element models can also be used for future parametric study as a reliable tool. More parameters such as the influence of fastener spacing, b/t ratio, steel section and concrete-filled contributions on composite column capacity, and composite column slenderness effects will be further investigated.

CRediT authorship contribution statement

Rohola Rahnavard: Preliminary design and planning of the experimental tests, Experimental tests and numerical modeling, Analytical study, Execution of experimental tests, Formal analysis and interpretation of the results, Writing – original draft. **Hélder D. Craveiro:** Funding acquisition, Supervision, Preliminary design and planning of the experimental tests, Formal analysis and interpretation of the results, Analytical study, Writing – review & editing. **Rui A. Simões:** Supervision, Formal analysis and interpretation of the results, Writing – review & editing. **Luís Laím:** Analytical study, Writing – review & editing. **Aldina Santiago:** Writing – review & editing.

Declaration of competing interest

The authors declare that they have no known competing financial interests or personal relationships that could have appeared to influence the work reported in this paper.

Data availability statement

The raw/processed data required to reproduce these findings cannot be shared at this time as the data also forms part of an ongoing study.

Acknowledgments

This work is financed by national funds through FCT - Foundation for Science and Technology, under grant agreement 2021.06528.BD attributed to the 1st author and under the grant agreement 2020.03588.CEECIND attributed to the 2nd author. The authors gratefully acknowledge to the Portuguese Foundation for Science and Technology (FCT) for its support under the framework of the research project PTDC/ECI-EGC/31858/2017 - INNOCFSCONC - Innovative hybrid structural solutions using cold-formed steel and lightweight concrete“, financed by FEDER funds through the Competitivity Factors Operational Programme - COMPETE and by national funds through FCT.

This work was partly financed by FCT/MCTES through national funds (PIDDAC) under the R&D Unit Institute for Sustainability and Innovation in Structural Engineering (ISISE), under reference UIDB/04029/2020.

The second author gratefully acknowledges the Portuguese Foundation for Science and Technology (FCT) for its support under the framework of the individual Scientific Employment Stimulus (CEECIND — 3rd Edition) program with reference 2020.03588. CEECIND.

Cofinanciado por:
COMPETE 2020 PROGRAMA OPERACIONAL COMPETITIVIDADE E INTERNACIONALIZAÇÃO
PORTUGAL 2020
UNIÃO EUROPEIA Fundo Europeu de Desenvolvimento Regional
FCT Fundação para a Ciência e a Tecnologia

References

[1] N.E. Shanmugam, B. Lakshmi, State of the art report on steel–concrete composite columns, J. Construct. Steel Res. 57 (10) (2001) 1041–1080, http://dx.doi.org/10.1016/S0143-974X(01)00021-9.

[2] An He, Fangying Wang, Ou Zhao, Experimental and numerical studies of concrete-filled high-chromium stainless steel tube (CFHSST) stub columns, Thin-Walled Struct. 144 (2019) 106273, http://dx.doi.org/10.1016/j.tws.2019.106273.

[3] Ben Young, Ehab Ellobody, Experimental investigation of concrete-filled cold-formed high strength stainless steel tube columns, J. Construct. Steel Res. 62 (5) (2006) 484–492, http://dx.doi.org/10.1016/j.jcsr.2005.08.004.

[4] Dennis Lam, Leroy Gardner, Structural design of stainless steel concrete filled columns, J. Construct. Steel Res. 64 (11) (2008) http://dx.doi.org/10.1016/j.jcsr.2008.04.012, 1275-1282.

[5] Fangying Wang, Ben Young, Leroy Gardner, Compressive behaviour and design of CFDST cross-sections with stainless steel outer tubes, J. Construct. Steel Res. 170 (2020) 105942, http://dx.doi.org/10.1016/j.jcsr.2020.105942.

[6] Brian Uy, Zhong Tao, Lin-Hai Han, Behaviour of short and slender concrete-filled stainless steel tubular columns, J. Construct. Steel Res. 67 (3) (2011) 360–378, http://dx.doi.org/10.1016/j.jcsr.2010.10.004.

[7] Zhong Tao, Zhi-Bin Wang, Qing Yu, Finite element modelling of concrete-filled steel stub columns under axial compression, J. Construct. Steel Res. 89 (2013) 121–131, http://dx.doi.org/10.1016/j.jcsr.2013.07.001.

[8] Jun Wang, Xianfeng Cheng, Chao Wu, Chuan-Chuan Hou, Analytical behavior of dodecagonal concrete-filled double skin tubular (CFDST) columns under axial compression, J. Construct. Steel Res. 162 (2019) 105743, http://dx.doi.org/10.1016/j.jcsr.2019.105743.

[9] Hongtuo Qi, Lanhui Guo, Jiepeng Liu, Dan Gan, Sumei Zhang, Axial load behavior and strength of tubed steel reinforced-concrete (SRC) stub columns, Thin-Walled Struct. 49 (9) (2011) 1141–1150, http://dx.doi.org/10.1016/j.tws.2011.04.006.

[10] Qingxiang Wang, Dazhou Zhao, Ping Guan, Experimental study on the strength and ductility of steel tubular columns filled with steel-reinforced concrete, Eng. Struct. 26 (7) (2004) 907–915, http://dx.doi.org/10.1016/j.engstruct.2004.02.009.

[11] Standards Australia. Bridge design, part 6: steel and composite construction. AS 5100.6-2004. Sydney (Australia), 2004.

[12] ANSI/AISC 360-05, Specification for Structural Steel Buildings, American Institute of Steel Construction, Chicago (IL, USA), 2005.

[13] DBJ/T 13-51-2010, Technical Specification for Concrete-Filled Steel Tubular Structures, The Department of Housing and Urban–Rural Development of Fujian Province, Fuzhou (China), 2010, (in Chinese).

[14] JGJ 138-2016, Code for Design of Composite Structures, Ministry of Housing and Urban-Rural Development of the People's Republic of China, China, 2016, (in Chinese).

[15] Eurocode 4, Design of Composite Steel and Concrete Structures, Part 1.1: General Rules and Rules for Building, BS EN 1994-1-1: 2004, British Standards Institution, London (UK), 2004.

[16] Meichun Zhu, Jianxin Liu, Qingxiang Wang, Xiufeng Feng, Experimental research on square steel tubular columns filled with steel-reinforced self-consolidating high-strength concrete under axial load, Eng. Struct. 32 (8) (2010) 2278–2286, http://dx.doi.org/10.1016/j.engstruct.2010.04.002.

[17] Yuyin Wang, Ligui Yang, Hua Yang, Changyong Liu, Behaviour of concrete-filled corrugated steel tubes under axial compression, Eng. Struct. 183 (2019) 475–495, http://dx.doi.org/10.1016/j.engstruct.2018.12.093.

[18] Wei Li, Qing-Xin Ren, Lin-Hai Han, Xiao-Ling Zhao, Behaviour of tapered concrete-filled double skin steel tubular (CFDST) stub columns, Thin-Walled Struct. 57 (2012) 37–48, http://dx.doi.org/10.1016/j.tws.2012.03.019.

[19] Jingming Cai, Jinlong Pan, Yufei Wu, Mechanical behavior of steel-reinforced concrete-filled steel tubular (SRCFST) columns under uniaxial compressive loading, Thin-Walled Struct. 97 (2015) 1–10, http://dx.doi.org/10.1016/j.tws.2015.08.028.

[20] Fa-xing Ding, Tao Zhang, Xue-mei Liu, Zhao-Hui Lu, Qiang Guo, Guo-shuai Jiang, Behavior of steel-reinforced concrete-filled square steel tubular stub columns under axial loading, Thin-Walled Struct. 119 (2017) 737–748, http://dx.doi.org/10.1016/j.tws.2017.07.021.

[21] Dan Gan, Zexiang Li, Tao Zhang, Xuhong Zhou, Kwok-fai Chung, Axial compressive behaviour of circular concrete-filled steel tubular stub columns with an inner bamboo culm, Structures 26 (2020) 156–168, http://dx.doi.org/10.1016/j.istruc.2020.04.016.

[22] Dilrukshie I. Samarakkody, David P. Thambiratnam, Tommy H.T. Chan, Praveen H.N. Moragaspitiya, Differential axial shortening and its effects in high rise buildings with composite concrete filled tube columns, Constr. Build. Mater. 143 (2017) 659–672, http://dx.doi.org/10.1016/j.conbuildmat.2016.11.091.

[23] Xuhong Zhou, Jiepeng Liu, Xuanding Wang, Y. Frank Chen, Behavior and design of slender circular tubed-reinforced-concrete columns subjected to eccentric compression, Eng. Struct. 124 (2016) 17–28, http://dx.doi.org/10.1016/j.engstruct.2016.05.036.

[24] Yue-Ling Long, Wen-Tao Li, Jian-Guo Dai, Leroy Gardner, Experimental study of concrete-filled CHS stub columns with inner FRP tubes, Thin-Walled Struct. 122 (2018) 606–621, http://dx.doi.org/10.1016/j.tws.2017.10.046.

[25] Jiepeng Liu, Jasim Ali Abdullah, Sumei Zhang, Hysteretic behavior and design of square tubed reinforced and steel reinforced concrete (STRC and/or STSRC) short columns, Thin-Walled Struct. 49 (7) (2011) 874–888, http://dx.doi.org/10.1016/j.tws.2011.02.012.

[26] Xuhong Zhou, Biao Yan, Jiepeng Liu, Behavior of square tubed steel reinforced-concrete (SRC) columns under eccentric compression, Thin-Walled Struct. 91 (2015) 129–138, http://dx.doi.org/10.1016/j.tws.2015.01.022.

[27] Hua Yang, Faqi Liu, Tak-ming Chan, Wei Wang, Behaviours of concrete-filled cold-formed elliptical hollow section beam–columns with varying aspect ratios, Thin-Walled Struct. 120 (2017) 9–28, http://dx.doi.org/10.1016/j.tws.2017.08.018.

[28] Jian-guo Nie, Yu-hang Wang, Jian-sheng Fan, Experimental study on seismic behavior of concrete filled steel tube columns under pure torsion and compression–torsion cyclic load, J. Construct. Steel Res. 79 (2012) 115–126, http://dx.doi.org/10.1016/j.jcsr.2012.07.029.

[29] M.F. Hassanein, Yong-Bo Shao, M. Elchalakani, A.M. El Hadidy, Flexural buckling of circular concrete-filled stainless steel tubular columns, Mar. Struct. 71 (2020) 102722, http://dx.doi.org/10.1016/j.marstruc.2020.102722.

[30] M.F. Hassanein, M. Elchalakani, V.I. Patel, Overall buckling behaviour of circular concrete-filled dual steel tubular columns with stainless steel external tubes, Thin-Walled Struct. 115 (2017) 336–348, http://dx.doi.org/10.1016/j.tws.2017.01.035.

[31] M.F. Hassanein, O.F. Kharoob, Analysis of circular concrete-filled double skin tubular slender columns with external stainless steel tubes, Thin-Walled Struct. 79 (2014) 23–37, http://dx.doi.org/10.1016/j.tws.2014.01.008.

[32] M.F. Hassanein, O.F. Kharoob, Compressive strength of circular concrete-filled double skin tubular short columns, Thin-Walled Struct. 77 (2014) 165–173, http://dx.doi.org/10.1016/j.tws.2013.10.004.

[33] M.F. Hassanein, O.F. Kharoob, Q.Q. Liang, Circular concrete-filled double skin tubular short columns with external stainless steel tubes under axial compression, Thin-Walled Struct. 73 (2013) 252–263, http://dx.doi.org/10.1016/j.tws.2013.08.017.

[34] M.F. Hassanein, M. Elchalakani, A. Karrech, V.I. Patel, Bo Yang, Behaviour of concrete-filled double-skin short columns under compression through finite element modelling: SHS outer and SHS inner tubes, Structures (ISSN: 2352-0124) 14 (2018) 358–375, http://dx.doi.org/10.1016/j.istruc.2018.04.006.

[35] Mohamed Elchalakani, M.F. Hassanein, Ali Karrech, Bo Yang, Experimental investigation of rubberised concrete-filled double skin square tubular columns under axial compression, Eng. Struct. 171 (2018) 730–746, http://dx.doi.org/10.1016/j.engstruct.2018.05.123.

[36] M.F. Hassanein, O.F. Kharoob, L. Gardner, Behaviour and design of square concrete-filled double skin tubular columns with inner circular tubes, Eng. Struct. (ISSN: 0141-0296) 100 (2015) 410–424, http://dx.doi.org/10.1016/j.engstruct.2015.06.022.

[37] M.F. Hassanein, O.F. Kharoob, Q.Q. Liang, Behaviour of circular concrete-filled lean duplex stainless steel–carbon steel tubular short columns, Eng. Struct. 56 (2013) 83–94, http://dx.doi.org/10.1016/j.engstruct.2013.04.016.

[38] M.F. Hassanein, V.I. Patel, Round-ended rectangular concrete-filled steel tubular short columns: FE investigation under axial compression, J. Construct. Steel Res. 140 (2018) 222–236, http://dx.doi.org/10.1016/j.jcsr.2017.10.030.

[39] M.A. Dabaon, M.H. El-Boghdadi, M.F. Hassanein, Experimental investigation on concrete-filled stainless steel stiffened tubular stub columns, Eng. Struct. 31 (2) (2009) 300–307, http://dx.doi.org/10.1016/j.engstruct.2008.08.017.

[40] Mohamed Dabaon, Saher El-Khoriby, Mahmoud El-Boghdadi, Mostafa Fahmi Hassanein, Confinement effect of stiffened and unstiffened concrete-filled stainless steel tubular stub columns, J. Construct. Steel Res. 65 (8–9) (2009) 1846–1854, http://dx.doi.org/10.1016/j.jcsr.2009.04.012.

[41] Ming-Xiang Xiong, De-Xin Xiong, J.Y. Richard Liew, Axial performance of short concrete filled steel tubes with high- and ultra-high- strength materials, Eng. Struct. 136 (2017) 494–510, http://dx.doi.org/10.1016/j.engstruct.2017.01.037.

[42] Ming-Xiang Xiong, De-Xin Xiong, J.Y. Richard Liew, Behaviour of steel tubular members infilled with ultra high strength concrete, J. Construct. Steel Res. 138 (2017) 168–183, http://dx.doi.org/10.1016/j.jcsr.2017.07.001.
[43] Ming-Xiang Xiong, De-Xin Xiong, J.Y. Richard Liew, Flexural performance of concrete filled tubes with high tensile steel and ultra-high strength concrete, J. Construct. Steel Res. 132 (2017) 191–202, http://dx.doi.org/10.1016/j.jcsr.2017.01.017.
[44] Sina Kazemzadeh Azad, Dongxu Li, Brian Uy, Axial slenderness limits for austenitic stainless steel-concrete composite columns, J. Construct. Steel Res. 166 (2020) 105856, http://dx.doi.org/10.1016/j.jcsr.2019.105856.
[45] Sina Kazemzadeh Azad, Brian Uy, Effect of concrete infill on local buckling capacity of circular tubes, J. Construct. Steel Res. 165 (2020) 105899, http://dx.doi.org/10.1016/j.jcsr.2019.105899.
[46] Sina Kazemzadeh Azad, Dongxu Li, Brian Uy, Axial slenderness limits for duplex and lean duplex stainless steel-concrete composite columns, J. Construct. Steel Res. 172 (2020) 106175, http://dx.doi.org/10.1016/j.jcsr.2020.106175.
[47] Lin-Hai Han, Zhong Tao, Hong Huang, Xiao-Ling Zhao, Concrete-filled double skin (SHS outer and CHS inner) steel tubular beam–columns, Thin-Walled Struct. 42 (9) (2004) 1329–1355, http://dx.doi.org/10.1016/j.tws.2004.03.017.
[48] Lin-Hai Han, Qing-Xin Ren, Wei Li, Tests on stub stainless steel–concrete–carbon steel double-skin tubular (DST) columns, J. Construct. Steel Res. 67 (3) (2011) 437–452, http://dx.doi.org/10.1016/j.jcsr.2010.09.010.
[49] Brian Uy, Zhong Tao, Lin-Hai Han, Behaviour of short and slender concrete-filled stainless steel tubular columns, J. Construct. Steel Res. 67 (3) (2011) 360–378, http://dx.doi.org/10.1016/j.jcsr.2010.10.004.
[50] Wei Li, Qing-Xin Ren, Lin-Hai Han, Xiao-Ling Zhao, Behaviour of tapered concrete-filled double skin steel tubular (CFDST) stub columns, Thin-Walled Struct. 57 (2012) 37–48, http://dx.doi.org/10.1016/j.tws.2012.03.019.
[51] Fa-cheng Wang, Lin-hai Han, Wei Li, Analytical behavior of CFDST stub columns with external stainless steel tubes under axial compression, Thin-Walled Struct. 127 (2018) 756–768, http://dx.doi.org/10.1016/j.tws.2018.02.021.
[52] Ehab Ellobody, Ben Young, Dennis Lam, Behaviour of normal and high strength concrete-filled compact steel tube circular stub columns, J. Construct. Steel Res. 62 (7) (2006) 706–715, http://dx.doi.org/10.1016/j.jcsr.2005.11.002.
[53] Ehab Ellobody, Ben Young, Numerical simulation of concrete encased steel composite columns, J. Construct. Steel Res. 67 (2) (2011) 211–222, http://dx.doi.org/10.1016/j.jcsr.2010.08.003.
[54] Ehab Ellobody, Ben Young, Dennis Lam, Eccentrically loaded concrete encased steel composite columns, Thin-Walled Struct. 49 (1) (2011) 53–65, http://dx.doi.org/10.1016/j.tws.2010.08.006.
[55] Dennis Lam, Leroy Gardner, Structural design of stainless steel concrete filled columns, J. Construct. Steel Res. 64 (11) (2008) 1275–1282, http://dx.doi.org/10.1016/j.jcsr.2008.04.012.
[56] Georgios Giakoumelis, Dennis Lam, Axial capacity of circular concrete-filled tube columns, J. Construct. Steel Res. 60 (7) (2004) 1049–1068, http://dx.doi.org/10.1016/j.jcsr.2003.10.001.
[57] S. Afshan, L. Gardner, The continuous strength method for structural stainless steel design, Thin-Walled Struct. 68 (2013) 42–49, http://dx.doi.org/10.1016/j.tws.2013.02.011.
[58] Fangying Wang, Ben Young, Leroy Gardner, Compressive behaviour and design of CFDST cross-sections with stainless steel outer tubes, J. Construct. Steel Res. 170 (2020) 105942, http://dx.doi.org/10.1016/j.jcsr.2020.105942.
[59] Fangying Wang, Ben Young, Leroy Gardner, Compressive testing and numerical modelling of concrete-filled double skin CHS with austenitic stainless steel outer tubes, Thin-Walled Struct. 141 (2019) 345–359, http://dx.doi.org/10.1016/j.tws.2019.04.003.
[60] Fangying Wang, Ben Young, Leroy Gardner, CFDST sections with square stainless steel outer tubes under axial compression: Experimental investigation, numerical modelling and design, Eng. Struct. 207 (2020) 110189, http://dx.doi.org/10.1016/j.engstruct.2020.110189.
[61] Abaqus Analysis User's Guide, Version 6.17, Dassault Systèmes Simulia, USA, 2017.
[62] EN 1993-1-3:2004, Eurocode 3: Design of Steel Structures, Part 1–3: General Rules, Supplementary Rules for Cold-Formed Members and Sheeting, European Committee For Standardization, Brussels, Belgium, p. 125.
[63] BS EN 10346:2009 - Continuously hot-dip coated steel flat products, Technical delivery conditions.
[64] EN ISO 6892-1:2006, Metallic Materials — Tensile Testing Part 1: Method of Test at Room Temperature, British Standards Institution, London, 2016.
[65] BS EN 206-1:2013, Concrete. Specification, Performance, Production and Conformity, British standards Institution, London, 2013.
[66] EN 1992-1-1, (English): Eurocode 2: Design of Concrete Structures - Part 1-1: General Rules and Rules for Buildings, 2004.
[67] Marko Pavlović, Zlatko Marković, Milan Veljković, Dragan Buđevac, Bolted shear connectors vs. headed studs behaviour in push-out tests, J. Construct. Steel Res. 88 (2013) 134–149, http://dx.doi.org/10.1016/j.jcsr.2013.05.003.
[68] Rohola Rahnavard, Carlos Rebelo, Hélder D. Craveiro, Rebecca Napolitano, Numerical investigation of the cyclic performance of reinforced concrete frames equipped with a combination of a rubber core and a U-shaped metallic damper, Eng. Struct. 225 (2020) 111307, http://dx.doi.org/10.1016/j.engstruct.2020.111307.
[69] Rohola Rahnavard, Carlos Rebelo, Hélder D. Craveiro, Rebecca Napolitano, Understanding the cyclic performance of composite steel-concrete connections on steel bridges, Eng. Struct. 224 (2020) 111213, http://dx.doi.org/10.1016/j.engstruct.2020.111213.
[70] D. Lam, X.H. Dai, L.H. Han, Q.X. Ren, W. Li, Behaviour of inclined, tapered and STS square CFST stub columns subjected to axial load, Thin-Walled Struct. 54 (2012) 94–105, http://dx.doi.org/10.1016/j.tws.2012.02.010.
[71] Rohola Rahnavard, Hélder D. Craveiro, Luís Laím, Rui A. Simões, Rebecca Napolitano, Numerical investigation on the composite action of cold-formed steel built-up battened columns, Thin-Walled Struct. 162 (2021) 107553, http://dx.doi.org/10.1016/j.tws.2021.107553.
[72] Hélder David da Silva Craveiro, Fire Resistance of Cold-Formed Steel Columns (PHD thesis), ISISE-Department of Civil Engineering, University of Coimbra, Portugal, 2016.
[73] Hélder D. Craveiro, Rohola Rahnavard, Rui A. Simões, Luís Laím, Aldina Santiago, Buckling behavior of closed built-up cold-formed steel columns under compression, Thin-Walled Struct. (2021) (TWST-D-21-01389 - under review).
[74] EN 1993-1-1, (English): Eurocode 3: Design of Steel Structures - Part 1-1: General Rules and Rules for Buildings, 2005.
[75] EN Eurocode3: Design of Steel Structures - Part 1-5: Plated Structural Elements. EN 1993-1-5. Brussels, 2006.
[76] AISC, Load and Resistance Factor Design Specification for Structural Steel Buildings, AISC Specification, American Institute of Steel Construction, Chicago, 1999.
[77] NAS, Specification for the Design of Cold-Formed Steel Structural Members, North American Cold-Formed Steel Specification, American Iron and Steel Institute, Washington, DC, 2001.